Lyu *et al. Biochar* (2026) 8:56
https://doi.org/10.1007/s42773-026-00573-4

Biochar

ORIGINAL RESEARCH Open Access

Contrasting effects of three aging processes on arsenic immobilization in red versus black soils amended by cerium-manganese modified biochar: the unique role of freeze–thaw cycling in governing arsenic fate at micro/nano interfaces

Peng Lyu[1,2], Xiaoya Huang[1,2], Lianfang Li[2*] and Yan Jiao[1]

Abstract

The aging mechanisms of modified biochar for arsenic (As) immobilization at micro/nano-interfacial scales in diverse soils remain poorly understood. Herein, we employed three aging treatments, including natural aging (NA), freeze–thaw cycles (FT), and dry–wet alternation (DW), to simulate the aging behavior of cerium-manganese modified biochar (CMBC) in two As-contaminated field soils. Results indicated that CMBC amendment significantly reduced soil pH by 7.5–16.7%, while simultaneously increasing dissolved organic carbon contents by 10–45%, available phosphorus levels by 11–43%, and the activities of four soil enzymes by 30–320% in comparison to unamended soils. These improvements proved to be most effective under FT-aging, followed by DW-aging and NA-aging. FT-aging also led to the most pronounced reduction in water-soluble As concentrations ranging from 94 to 99%, as well as a decrease in As mobilization coefficients of 38% to 59% in CMBC-amended soils when compared to DW-aging and NA-aging. The superior As immobilization under FT-aging can be attributed to adhesion mediated by Ce–Si crystal nano-bridge between soil microparticles and CMBC matrix, whereas such adhesion was not observed in NA/DW-aged samples. This unique interfacial configuration promoted Ca/Fe-oxide intercalation and amorphous Ce-oxides formation within CMBC, which facilitated the development of As–Fe/Ce crystalline phases. Meanwhile, the synergistic enrichment of metallic and oxygen-containing groups on FT-aged CMBC surface induced the formation of stable As–Ce/Fe–O species and triggered dual redox transformations: (1) Ce/Mn reduction drove bulk As(III) oxidation to As(V), and (2) Fe(0) oxidation mediated partial reduction of As(V)/As(III) to inert As(0). Notably, CMBC-amended red soil exhibited preferential As immobilization during aging due to the tighter adhesion between nano-CMBC and soil colloids. This enhanced adhesion strengthened the bonding of Ce/Fe-oxides with As and intensified the oxidation of As(III) to As(V) through increased Ce/Mn reduction. This study provides innovative microscale mechanistic insights into the aging behavior of modified biochar for remediating diverse soils contaminated with potentially toxic elements.

*Correspondence:
Lianfang Li
lilianfang@caas.cn
Full list of author information is available at the end of the article

Springer

Highlights

- Aging mechanisms of modified biochar for As fate at micro-interface were studied.
- Treatment efficacy of soil properties and As immobilization was ranked as FT>DW>NA.
- Ce/Si nano-bridge mediated CMBC-soil colloid adhesion was first found in FT-aging.
- Interfacial restructuring promotes stable As–Fe/Ce–O development and dual As redox.
- Red soil aging enhances immobilization via tighter CMBC-soil colloids adhesion.

Keywords Modified biochar, Aging mechanism, Arsenic fate, Freeze–thaw cycling, Soil micro-interfaces

Graphical Abstract

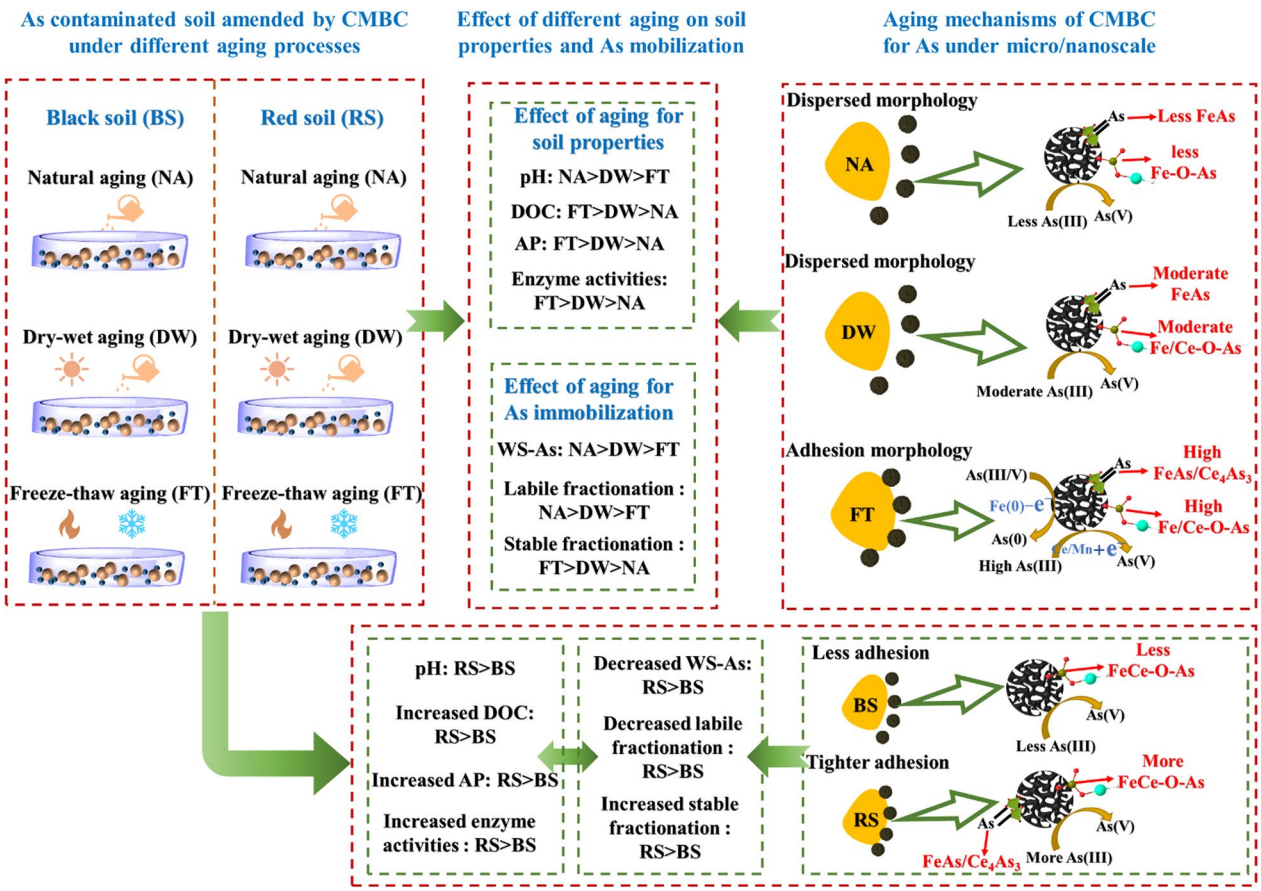

1 Introduction

Biochar, a carbon-rich porous substance produced through biomass pyrolysis or hydrothermal carbonization, possesses eco-friendly physicochemical properties, such as a large specific surface area (SSA), excellent biocompatibility, and abundant O-containing functional groups (Cowie 2023). These attributes make it widely applicable in soil remediation, carbon sequestration, and wastewater purification (Saraugi et al. 2025). In particular, biochar-based materials have garnered significant attention for immobilizing potentially toxic elements (PTEs) in contaminated soil. They can drive the phase transformation of soil mineral-PTE complexes, act as electron shuttles to facilitate redox reactions, and enhance the soil cation exchange capacity, thereby promoting exchange of PTEs with non-toxic ions (Sun et al. 2022; Wei et al. 2024). However, pristine biochar lacks essential metal-functional groups and possesses a

negatively charged surface, which limits its capacity for anionic PTE immobilization due to weak bonding interactions and electrostatic repulsion (Gong et al. 2022). This limitation is particularly evident with arsenic (As), a priority toxic contaminant associated with cancer, organ dysfunction, and hypertension upon long-term exposure (Cao et al. 2025; Wang and Liu 2024). To address these challenges, various surface-tailoring methodologies have been developed to enhance biochar adsorption and immobilization capacity for As, including modifications with metal-(oxyhydr)oxides, nonmetallic functionalization, and microorganism colonization (Lyu et al. 2024b; Ravindiran et al. 2024). Variable-valent metals like iron (Fe), manganese (Mn), and cerium (Ce) are preferred candidates for biochar modification, because of their abilities to participate in immobilization reactions with As through mechanisms such as redox, coordination, and precipitation (Ravindiran et al. 2024). In our previous study, Ce-Mn-modified biochar (CMBC) exhibited excellent As adsorption performance, which was attributed to the complexation of As with Ce-Mn metal bonds and co-precipitation involving Mn-oxide lattice defects (Liang et al. 2020). Nevertheless, it remains unclear whether CMBC can effectively immobilize As in diverse contaminated soils and how its aging behavior influences the fate and transformation of As in these environments.

Biochar undergoes natural physical, chemical, and microbiologically decay processes, collectively referred to as "aging", following its application to soil through interactions with soil components, sunlight, and microorganisms (Wang et al. 2020). These aging behaviors alter the physicochemical characteristics of biochar, such as SSA, microporous structure, and elemental composition (Yang et al. 2023). Such alterations may either enhance or impair the adsorption and immobilization performance of biochar for PTEs. Among various aging treatments, freeze–thaw and dry–wet cycles have received particular attention due to their prevalence in natural soil environments and significant impacts on the physicochemical properties of biochar. For example, dry–wet cycling has been shown to increase cadmium (Cd) mobilization in soil amended by $KMnO_4$-modified biochar compared to other aging treatments, primarily due to the massive loss of O-containing functional groups and pore clogging (Meng et al. 2022). Conversely, combined freeze–thaw and dry–wet aging enhanced Cd-π complexation and Cd precipitation in soil amended with MgO-modified biochar (Yang et al. 2024a). Regarding As, dry–wet aging reduced its bioavailability in soil amended with zero-valent iron (ZVI)-modified biochar due to ZVI dissolution, whereas freeze–thaw aging promoted As immobilization via the crystallization of amorphous Fe–As complexes (Zhang et al. 2022a). These studies highlight that freeze–thaw cycles and wet-dry alternations can drive distinct biogeochemical processes of PTEs and thus affect their transport and transformation in soil.

However, biochar aging performance and corresponding mechanisms are known to vary significantly across different soil types due to variations in soil composition and physicochemical properties (Long et al. 2024). Although some studies have explored how aging in diverse soils alters raw biochar characteristics, microcystin adsorption, and nitrate retention (Cao et al. 2017; Cooper et al. 2023; Yuan et al. 2021), the influences of these aging processes on the fates and bioavailabilities of PTEs in soils amended with modified biochar remain unclear. This knowledge gap is critical, particularly for major As-contaminated soils like black soil (BS) and red soil (RS), which serve as essential growing media for staple crops such as rice, wheat, and corn. Therefore, exploring the impacts of the aging process on the remediation of BS and RS soils by biochar materials is of significant importance for the remediation of PTE-contaminated soils. BS and RS soils differ significantly in physicochemical properties, including organic matter content, pH, redox potential, and mineralogical species (Guo et al. 2024). Consequently, modified biochar is expected to exhibit distinct aging behaviors in these soils, which can affect the effectiveness of PTE immobilization. This emphasizes the necessity for an in-depth investigation into the aging mechanisms of modified biochar in BS and RS soils to better understand its responses in different soil environments.

Biochar aging in soil alters its physicochemical properties and can fragment it into micro- and nano-sized particles (Long et al. 2024). Aging processes like freeze–thaw and wet–dry cycles compromise structural integrity through cracking, swelling, and pore collapse induced by heat release and water vapor (Liu et al. 2025; Zhao and Shang 2023). These morphological transformations generate micro/nano-biochar with distinct physicochemical characteristics, thereby modifying their heterogeneities to bind PTEs. Earlier studies report that aging treatments alter the chemisorption type of ramie nano-biochar while increasing its physical adsorption of Cd (Wang and Liu 2024). Moreover, aging increases the binding performance of micro/nano-biochar for As compared to bulk biochar, likely due to a stronger affinity of As(III) for humic-like components (Xu et al. 2024). However, these findings are primarily from simulated chemical environments, leaving the micro/nano-interfacial aging mechanisms that control As fate in real soils largely unknown.

To address these knowledge gaps, this study employed three aging treatments, including natural aging, freeze–thaw cycles, and dry–wet alternation, to simulate the CMBC aging in two real soils. The effects of these aging

treatments on key soil properties and As immobilization capacity of CMBC were investigated. Furthermore, the aging mechanisms of CMBC for As stabilization in soils were revealed using characterization techniques such as X-ray diffraction (XRD), Fourier-transform infrared spectroscopy (FT-IR), X-ray photoelectron spectra (XPS), among others. This research will provide critical insights into the role of modified biochar aging on the geochemical fate of As in real soils.

2 Materials and methods

2.1 Soil and reagent

The experimental soils used in this study were red soil (RS) and black soil (BS), collected from As-contaminated areas in China. The RS sample was sourced from farmland near the Shimen Realgar Mining Area in Hunan Province (29°39′27″ N, 111°31′12″ E), while the BS soil sample was obtained from the vicinity of the Dalian Dahua Chemical Plant in Liaoning Province (38°57′15″ N, 121°38′64″ E). The total As concentrations in BS and RS soils were 182.14 and 157.82 mg kg^{-1}, respectively, both exceeding the limit stipulated by Chinese national standard (GB 15618-2018). Other physicochemical properties of the soils are shown in Table S1. Analytically pure chemical reagents, such as $CeCl_3$, $KMnO_4$, HCl, were used for material preparation and chemical experiments. All reagents were purchased from Aladdin Chemistry Co. Ltd.

2.2 Preparation of CMBC

The optimal synthesis procedure of CMBC was based on our previous research (Liang et al. 2020). In brief, original biochar (BC) was prepared by anaerobic pyrolysis of wheat straw at 600 ℃ for 2 h. The BC was then thoroughly washed with 0.01 M HCl to remove impurities, following by washing with deionized water until the effluent reached a neutral pH. After drying, the BC powder was pre-impregnated with 0.6 M $CeCl_3$ and 0.3 M $KMnO_4$ at a mass ratio of 4:3:1 (BC:$CeCl_3$:$KMnO_4$) under magnetic stirring for 2 h. The mixture was then filtered and freeze-dried. The obtained solid was subjected to a second pyrolysis step under the same conditions (600 ℃ for 2 h) to yield the final product, which was designated as CMBC. The resulting CMBC was ground and sieved through a 100-mesh (0.125 mm) screen for subsequent application and characterization. The morphology, crystallography, specific surface area, and surface functional groups of CMBC have been reported previously (Liang et al. 2020).

2.3 Material aging treatments

CMBC was thoroughly mixed with 100 g of BS or RS soil, each with a particle size of 0.25 mm (60-mesh sieve), at mass ratios of 1%, 2.5%, and 5%. The resulting CMBC-soil mixtures were subjected to natural aging (NA), freeze–thaw cycles (FT), and wet–dry cycles (DW) incubation in beakers, where the NA-aging served as the control treatment. For NA, the mixtures were maintained at 70% soil moisture content and incubated at 25 ℃ for 30 d. The FT treatment underwent 30 cycles, each consisting of 12 h at −20 ℃ followed by 12 h at 25 ℃, with soil moisture was monitored and maintained at 70% throughout the 30-day period. For DW treatment, the mixtures were maintained at 100% moisture content and incubated at 25 ℃ for 16 h, followed by incubation at 65 ℃ for 8 h, during which the moisture content was allowed to decrease but remained above 30%. This process was repeated for 30 cycles. All beakers used in aging treatments were sealed with a film containing 5 small pores to maintain water–air balance. Unamended BS and RS soils were also subjected to the same aging treatments as described above. All soil aging treatments were conducted in triplicate.

2.4 Analysis of soil properties

Soil samples were collected at the 1st, 3rd, 7th, 15th, and 30th cycles during all aging treatments to evaluate dynamic indicators, including soil pH and water-soluble As (WS-As) content. At the end of all aging periods, the distribution of As species in soil was analyzed, along with the activities of soil enzymes including urease, catalase, alkaline phosphatase, and sucrase. Meanwhile, the contents of dissolved organic carbon (DOC) and available phosphorus (AP) in soil were measured. The distribution of As species was analyzed using the Wenzel sequential extraction method, which categorized them into five fractions: the non-specifically adsorbed fraction (F1), the specifically adsorbed fraction (F2), the fraction adsorbed on amorphous and poorly-crystalline hydrous oxides of Fe and Al (F3), the fraction adsorbed on crystalline hydrous oxides of Fe and Al (F4), and the residual phases (F5). The mobility of these species can be ranked as: F1 > F2 > F3 > F4 > F5 (Wenzel et al. 2001). Furthermore, to assess the leaching risks of Ce/Mn from CMBC into soil, we measured the bioavailable Ce/Mn concentrations via the acetic acid (0.1 M) extraction. Detailed methods for the detection of the above indicators, as well as the basic physicochemical properties of BS and RS soils, are provided in Text S1.

The immobilization efficiency (η) and mobilization coefficients (Mc) of As in soil were calculated using Eq. 1 and Eq. 2, respectively.

$$\eta(\%) = \frac{(C_0 - C_e)}{C_0} \times 100\% \quad (1)$$

$$Mc = \frac{F1 + F2}{F1 + F2 + F3 + F4 + F5} \quad (2)$$

where C_0 and C_e are the WS-As contents of soil with and without addition of CMBC, respectively.

2.5 Aging mechanism characterization of CMBC

At the end of each aging period, CMBC powder, which had been added at a 5% mass ratio and co-aged with the soils, was recovered. The recovery process involved an initial screening based on particle size differences (CMBC particle size: 0.125 mm and soil particle size: 0.25 mm), followed by manual selection of biochar particles using tweezers under a light microscope. The purified CMBC samples were then characterized using a series of analytical techniques. The morphologies and elemental distribution were characterized by a GeminiSEM 300 equipped with a Smartedx EDS spectra (ZEISS, Germany). The surface elemental composition and chemical states were analyzed using X-ray photoelectron spectroscopy (XPS) (Thermo Scientific K-Alpha, USA). Mineral crystal structures were identified by D8 Advance XRD with Cu Kα radiation (Bruker, Germany). Surface functional groups were characterized using an FT-IR spectrometer (Thermo Fisher Scientific Nicolet iS20, USA). The products of CMBC after NA-aging, FT-aging, and DW-aging were labeled as NA-CMBC, FT-CMBC, and DW-CMBC, respectively.

2.6 Statistical analysis

The experimental data were presented as the mean ± standard deviation of triplicates. One-way analysis of variance (ANOVA) and Duncan's multiple range tests were performed using SPSS Statistics version 20 software, with a significance level set at 0.05 (P), to evaluate significant differences in the mean values. The Pearson correlation coefficient was calculated to analyze the relationship between As mobilization coefficient and soil properties.

3 Results and discussion

3.1 Effect of different aging treatments on soil properties

3.1.1 Soil pH

Figure 1a, b exhibit the temporal changes in soil pH for control (CK) and CMBC-amended soils under different aging treatments. Overall, higher doses of CMBC treatment led to greater decreases in soil pH across all aging regimes. After 30 cycles, the pH in BS and RS soils amended with 5 wt% CMBC decreased by 7.5–8.6% and 6.3–16.7%, respectively, compared to the CK soil. This acidifying effect suggests that CMBC had a stronger alkaline soil buffering capacity, potentially favoring As immobilization by suppressing H^+ ion activity. Interestingly, this finding differs from previous studies in which similarly modified biochars were found to increase soil pH (Guo et al. 2025; Zhang et al. 2022b). This discrepancy may be attributed to the aging-induced release of acidic species (e.g., carboxyl and phenolic groups) from CMBC through H^+ activation and the production of low-molecular-weight organic acids, which can collectively weaken the acid-buffering capacity of soil (Long et al. 2024). However, the temporal pH variation in CMBC-amended soils depended on aging mode and soil type. In BS soil (Fig. 1a), pH decreased gradually under NA-aging, dropped rapidly under FT-aging, and increased initially before decreasing sharply under DW-aging. Therefore, the final pH values in 5 wt% CMBC-amended BS soil followed the order: NA-aging ≈ DW-aging > FT-aging (Fig. 1c). The dramatic temperature fluctuations during FT-aging likely accelerated the release of acidic functional groups from CMBC microparticle and soil organic matter, which subsequently reacted with cations to form carboxylates and phenolates that can produce H^+ ions (Xu et al. 2018). The initial pH increase under DW-aging was related to the dissolution of alkaline minerals from soil microaggregates (Liu et al. 2025).

In contrast to BS soil, the pH changes in CMBC-amended RS soil were less affected by aging types (Fig. 1b). The pH in RS generally exhibited an initial decrease followed by an increase, plateauing after 15 cycles. This behavior can be attributed to the significantly higher clay and silt contents in RS than those in BS (Table S1). The dense texture of these clay minerals maintains a stable structure against freeze–thaw and dry–wet stresses, thereby limiting the release of H^+ and OH^- ions from soil colloids. Similar to the trend observed in BS soil, the final pH of RS soil amended with 5 wt% CMBC under FT-aging was significantly lower ($p < 0.05$) than under NA- or DW-aging (Fig. 1d). This reflects that FT-aging promotes the release of positively charged protons, which would induce the electrostatic attraction of As and facilitate its stabilization.

3.1.2 Dissolved organic carbon and available phosphorus

Figure 2a exhibits a comparison of DOC contents in differentially treated soils after 30 aging cycles. As anticipated, CMBC amendment elevated DOC concentrations under all aging treatments, increasing them by 10–35% in BS soil and 5–45% in RS soil relative to unamended soil. This enhancement is likely attributed to the slow release of O-containing functional groups and low-molecular-weight organic acids from the CMBC matrix (Long et al. 2024). In fact, these labile organic matters are highly responsive to soil environment perturbations. For example, the temperature-humidity fluctuations can induce the release of exogenous

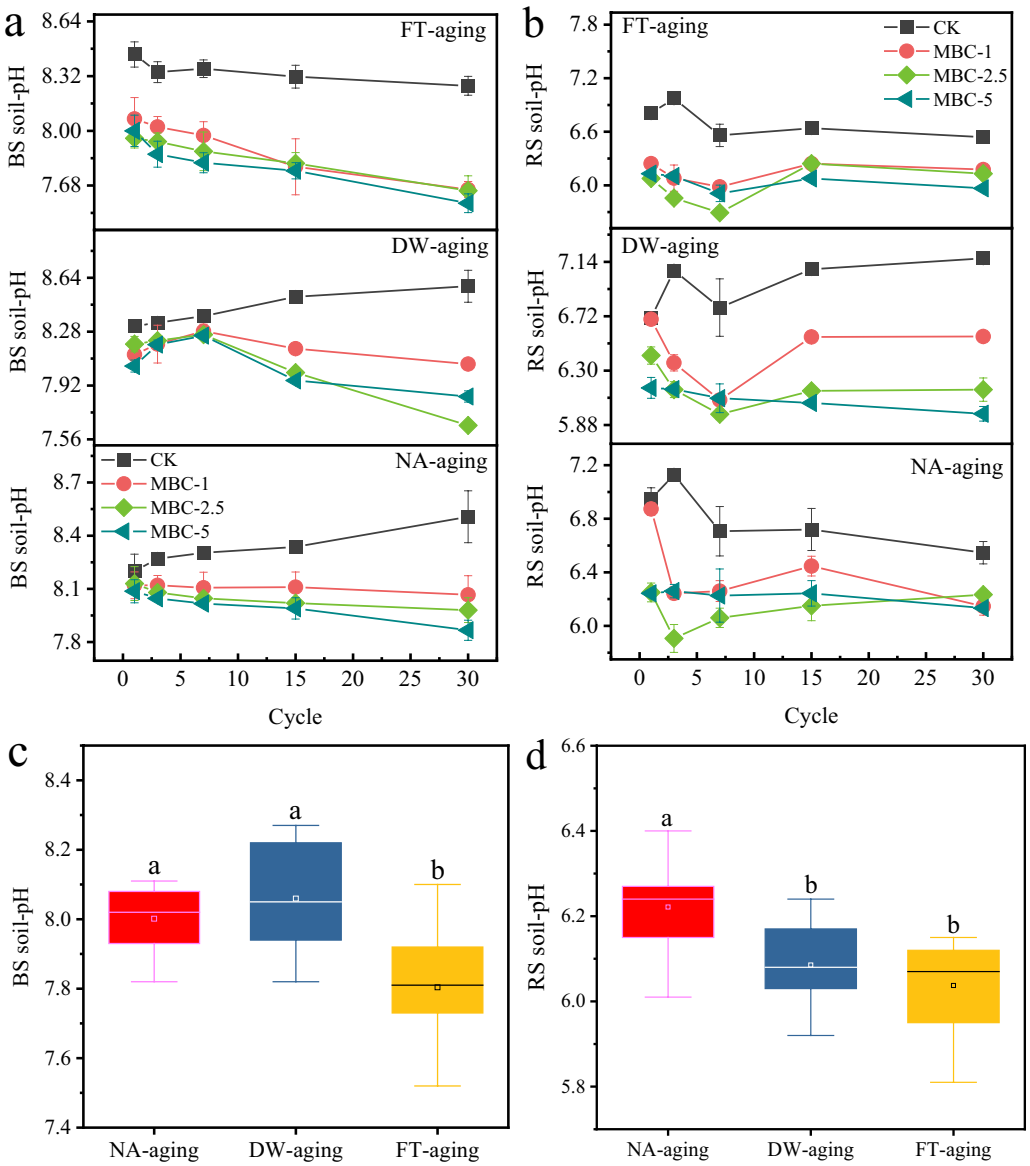

Fig. 1 Temporal changes in soil pH under different aging treatments in **a** BS and **b** RS soils. Comparison of pH in **c** BS and **d** RS soils treated with 5% dose of CMBC during diverse aging treatments. CK represents the control treatment, CMBC-1, 2.5, or 5 represents the 1%, 2.5%, or 5% mass ratio of CMBC amendment to soil. NA-, DW-, and FT-aging refer to natural aging, dry–wet alternation, and freeze–thaw cycling, respectively. Different lowercase letters above each bar in **c**, **d** indicate a significant difference ($p < 0.05$) between different treatments

organic inputs such as plant-animal residues, humic substances, and soil necromass (Luo et al. 2023). As a result, both amended and unamended soils exhibited significantly higher DOC contents after DW- and FT-aging than after NA-aging. Specifically, in soils amended with 5 wt% CMBC, DOC contents were 4–7% higher under DW-aging and 20–43% higher under FT-aging compared to NA-aging. The more pronounced DOC accumulation under FT-aging underscores its pivotal role in the formation of carbon sinks. This may arise from the thermally driven transformation of biochar-derived aromatic components into labile organic matter and organic acids, along with the enhanced dissolution of organic complexes during intense freeze–thaw cycles (Yang et al. 2023). DOC is critical for immobilizing soil contaminants like As through complexation with low-molecular-weight organic acids, interactions with organic matter, and electron shuttling via humic substances (Si et al. 2024). Therefore, the significant rise in DOC under FT-aging likely contributes to

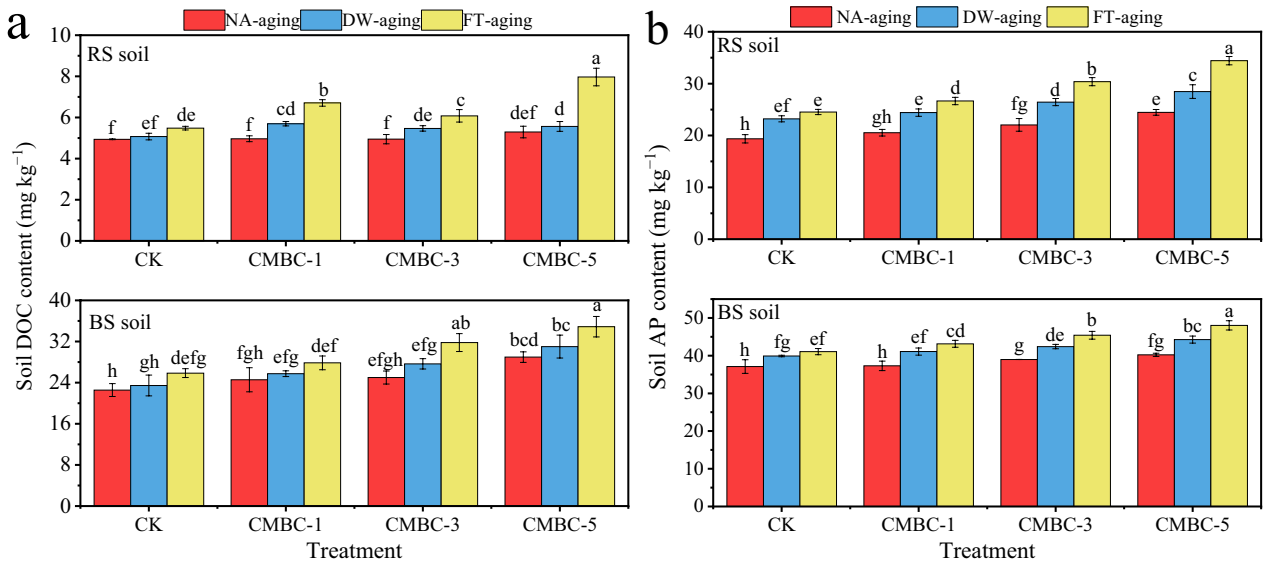

Fig. 2 Effect of different aging treatments on the concentrations of **a** dissolved organic carbon and **b** available phosphorus in unamended and CMBC-amended BS and RS soils. Different lowercase letters above each bar indicate a significant difference ($p < 0.05$) between different treatments

the enhanced As immobilization observed in CMBC-amended soils (Fig. 4).

As shown in Fig. 2b, the AP contents in both soils increased dose-dependently with higher CMBC amendment levels across all aging processes, demonstrating an enhanced effect of CMBC for phosphorus retention. This effect likely stems from the high specific surface area and strong complexation capacities of Ce/Mn-oxides within CMBC, which facilitate phosphorus adsorption and stabilize soil phosphorus pools (Gong et al. 2024). Notably, the AP content in CMBC-amended soils followed the order: FT-aging > DW-aging > NA-aging. The increase in AP under DW- and FT-aging may be due to the weathering of mineral-bound phosphorus and accelerated mineralization of organic phosphorus via temperature-humidity cycling (Yadav et al. 2019). Meanwhile, the aging-induced increase in phosphatase activity (Fig. 3d) could further promote the hydrolysis of phosphomonoesters/diesters into inorganic phosphorus (Sun et al. 2021). The positive influences of CMBC addition and FT-aging on AP levels likely induce the As mobilization due to the competition between phosphate (a chemical analogue of arsenate) and As for bonding sites on soil minerals. However, our results showed an enhanced immobilization of As under FT-aging with CMBC amendment (Fig. 4). This discrepancy can be attributed to the multiple encapsulation mechanisms for As, including As-Mn/Ce complexation and As-mineral-bearing precipitation, which can overcome the competitive adsorption of phosphate (Lyu et al. 2024a). Interestingly, RS soil displayed greater sensitivity to FT-aging than BS soil in both DOC and AP contents under CMBC amendment. Specifically, RS soil showed increases of 11–43% in DOC and 37–41% in AP, whereas BS soil exhibited narrower ranges of 10–20% for DOC and 16–20% for AP. This differential responsiveness likely reflects the inherently higher iron-(oxyhydr)oxide level in Krasnozem-derived RS soils, where repetitive freeze–thaw promote reductive dissolution of Fe(III) phases, thereby liberating mineral-bound organic matter and phosphorus into the dissolved phase (Wang et al. 2025).

3.1.3 Enzyme activity of soil

Soil enzyme activity is an integrative bioindicator of soil fertility and nutrient availability. As shown in Fig. 3, the activities of catalase, urease, sucrase, and alkaline phosphatase showed a more pronounced positive response to higher doses of CMBC across all aging processes. Specifically, compared to CK, the activities of these four enzymes increased by 30–250% in BS and 40–320% in RS soil amended with 5 wt% CMBC. The beneficial effects of CMBC on enzyme activities are associated with its large specific surface area and porous structure, which provide habitats and nutrients (e.g., organic carbon, phosphorus, nitrogen) for soil microorganisms (Manasa et al. 2020). Similar studies have been reported by Shao et al. (2023) and Wang et al. (2022), who found significant enhancements in the activities of alkaline phosphatase, catalase, and urease in contaminated soils amended with phosphorus-loaded biochar and layered

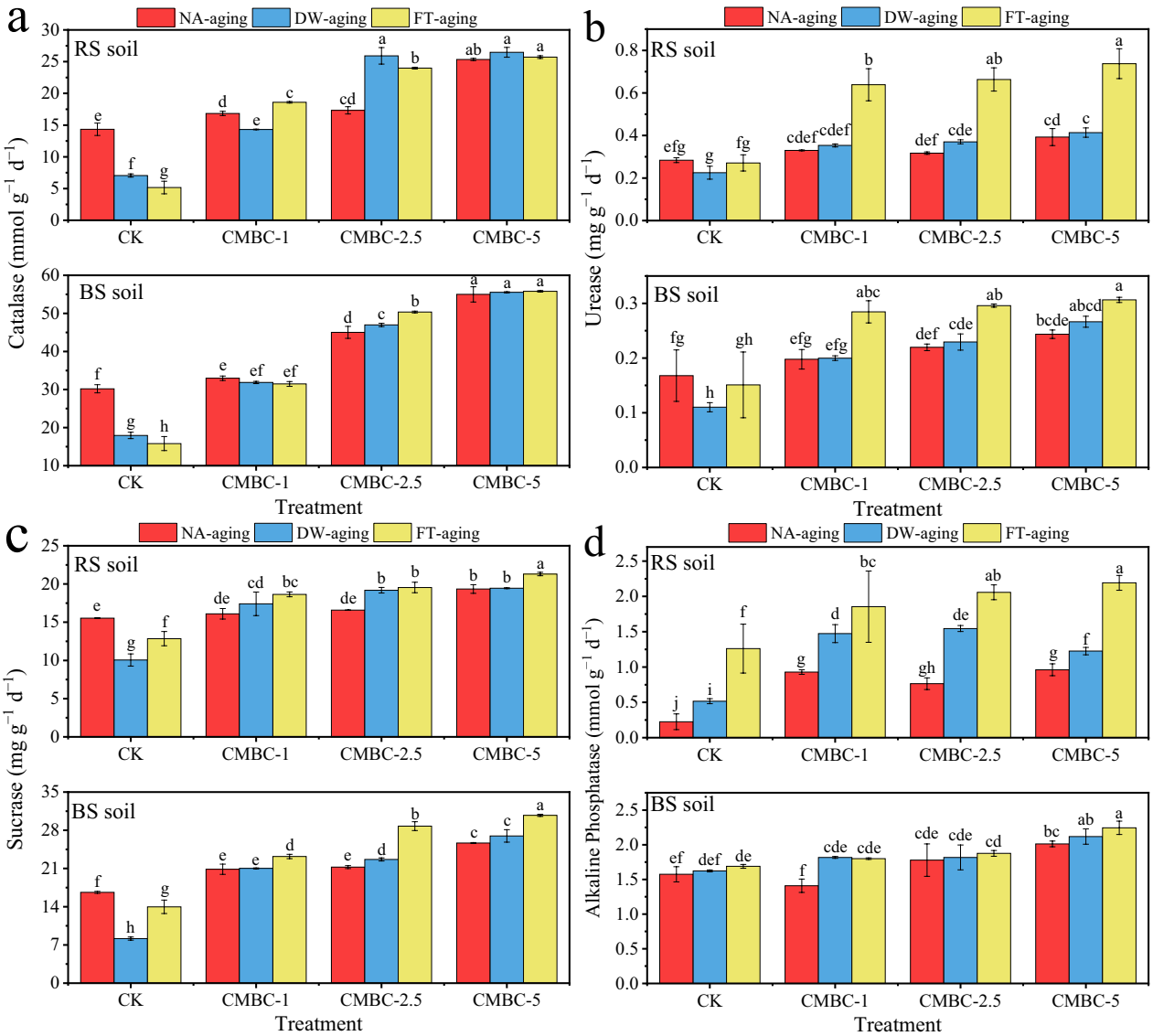

Fig. 3 Effect of different aging treatments on activities of **a** catalase, **b** urease, **c** sucrase, and **d** alkaline phosphatase in unamended and CMBC-amended BS and RS soils. Different lowercase letters above each bar indicate a significant difference ($p < 0.05$) between different treatments

double hydroxide-modified biochar. In contrast, some studies have noted that raw biochars can inhibit soil enzyme activities due to the oxidative stress caused by free radicals and their limited ability to alleviate the toxicities of PTEs (Shao et al. 2023; Yang et al. 2021). The positive influence observed in this study implies that Ce/Mn modification not only mitigates the oxidative stress of fresh biochar on soil microorganisms but also reduces As-induced toxic stress on enzyme substrates.

The effect of different aging treatments on enzyme activities in both amended BS and RS soils generally followed the order of FT-aging > DW-aging > NA-aging. The pronounced stimulatory impact of FT-aging on enzyme activities can be ascribed to the apoptosis and lysis of bacteria and fungi, which release intracellular components that support the growth of surviving microorganisms. Additionally, the repetitive expansion and contraction during freeze–thaw cycles induce fragmentation of soil aggregates and expose bioavailable sites, thereby promoting the growth of surviving microorganisms (Yang et al. 2021). Similarly, Yadav et al. (2019) observed that a short-term aging treatment increased the activities of dehydrogenase, phosphatase, and urease in soil amended with biochar.

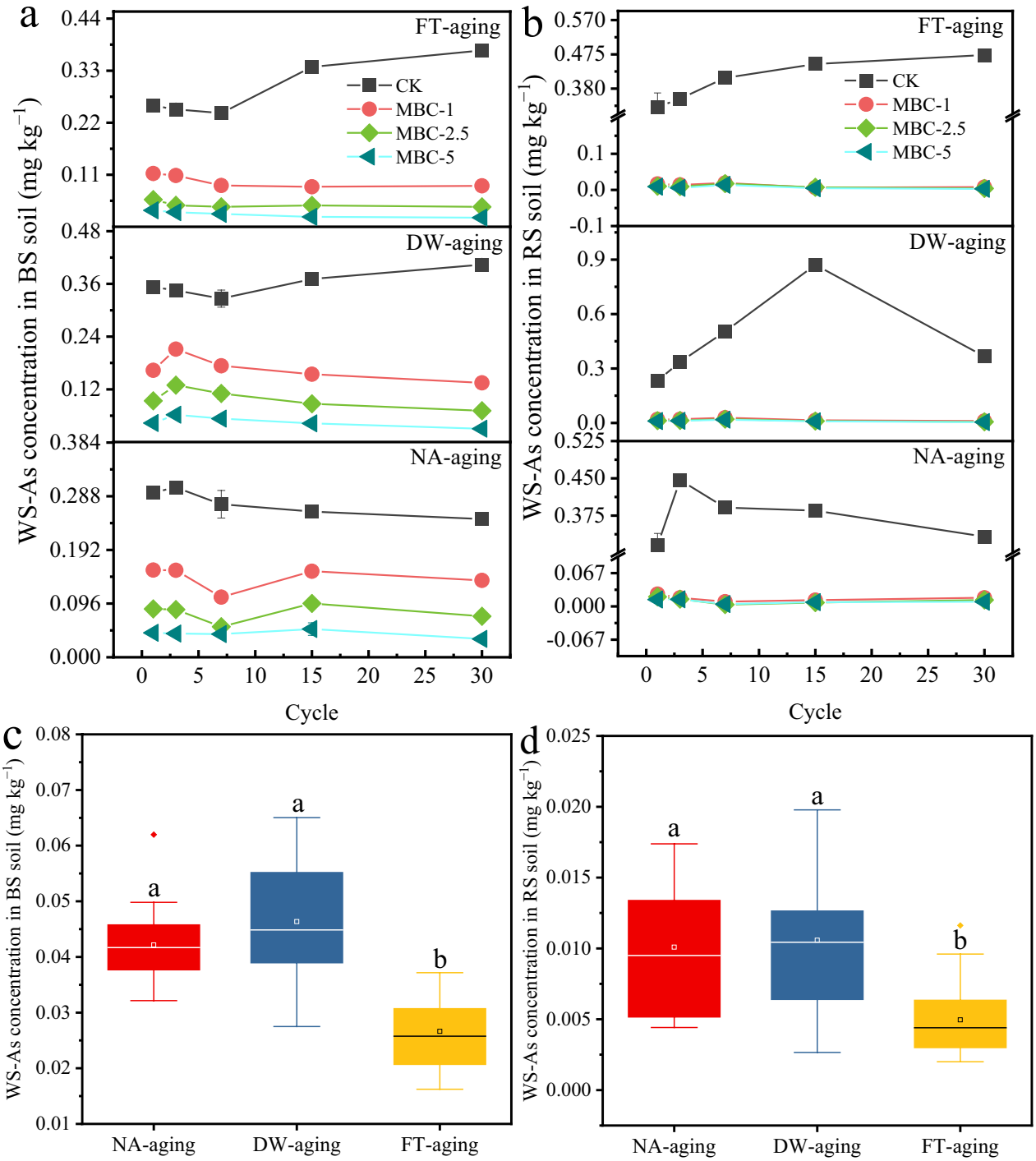

Fig. 4 Temporal changes in WS-As concentration of control and CMBC-remediated soil under different aging treatments in **a** BS and **b** RS soils. Comparison of WS-As concentrations in **c** BS and **d** RS soils treated with 5% dose of CMBC during different aging treatments. CK represents the control treatment, CMBC-1, 2.5, and 5, respectively represent the 1%, 2.5%, and 5% mass ratio of CMBC amendment to soil. NA-, DW-, and FT-aging refer to natural aging, dry–wet alternation, and freeze–thaw cycling, respectively. Different lowercase letters above each bar in **c**, **d** indicate a significant difference ($p < 0.05$) between different treatments

In CMBC-treated soils, the differences in catalase, urease, and sucrase activities between NA-aging and DW-aging were minimal, while these enzyme activities were significantly lower under DW-aging than under NA-aging in unamended BS and RS soils. The slightly or markedly inhibitory effect of DW-aging is likely due to the combined heat and moisture stress during the high-temperature phase, which can denature and degrade extracellular enzymes (Liao et al. 2025). Notably, the increases in urease and alkaline phosphatase activities with CMBC amendment were significantly higher ($p < 0.05$) in RS soil than in BS soil (Fig. 3b, d), implying a more sensitive microbial response in RS soil. Causally, the higher N and P levels in BS soil increase the substrate sources for these two enzymes, which results in a lower threshold for the increase in enzyme activity caused by CMBC remediation.

3.2 Effect of different aging treatments on As immobilization

3.2.1 The change in water-soluble As

The temporal changes in water-soluble As (WS-As) concentrations in unamended and CMBC-amended soils under different aging treatments are shown in Fig. 4a, b. Similar to the trends observed for soil pH, higher doses of CMBC amendment decreased WS-As concentrations across all aging treatments, highlighting the effectiveness of CMBC in As immobilization. However, the temporal variations in WS-As concentrations of CMBC-amended soils varied with aging treatment and soil type. In BS soil (Fig. 4a), WS-As concentrations under NA-aging initially decreased, then increased, and eventually plateaued at 30 cycles. Under DW-aging, WS-As concentrations first increased and then gradually decreased. In contrast, FT-aging led to a continuous decline in WS-As, which stabilized after 30 cycles. This pattern indicates that FT-aging contributes to persistent As immobilization in CMBC-remediated soil. Moreover, the final WS-As concentrations in 5 wt% CMBC-treated soils under FT-aging were significantly lower ($p < 0.05$) than those under DW- and NA-aging (Fig. 4c, d).

The enhanced As retention under FT-aging may be attributed to localized fractures in the biochar matrix of CMBC, which generate additional micropores and mesopores, thereby increasing the available adsorption sites on CMBC surface (Wang and Liu 2024). Furthermore, the lowest soil pH under FT-aging can result in significant electrostatic attraction of As. Lower pH level is often associated with higher redox potential (Eh), which facilitates the oxidation of As(III) to less mobile forms (Honma et al. 2016). Previous studies also reported that the collapse of recalcitrant soil minerals during FT-aging led to the formation of organo-mineral micro-agglomerates and organic plaque layers, which, with their abundant O-containing functional groups and well-developed micropores, promoted strong coprecipitation and complexation of PTEs such as As, Ni, and Cd (Long et al. 2024; Yang et al. 2021). Interestingly, WS-As concentrations in CMBC-amended RS soil decreased gradually over time and were less affected by aging types or doses (Fig. 3b), implying an inherent preference for As immobilization in RS soil. This aligns with previous studies that reported higher passivation capacities for As, Cd, and Pb using stabilizers in Krasnozem soil (Wei et al. 2024). Causally, a significantly higher poorly crystalline Fe and Al oxide-bound As was observed in unamended RS soil (Fig. 4b). As a result, the interaction between metastable As in RS soil and the active metal species and surface O-containing functional groups on CMBC likely facilitates As immobilization in weakly alkaline environments (Honma et al. 2016).

At the end of aging processes, the WS-As concentrations in BS and RS soils amended with 5 wt% CMBC decreased by 86–94% and 97–99%, respectively, compared to the CK soil. The immobilization efficiencies of CMBC for As under different aging treatments were further compared with findings from recent studies. As shown in Table 1, most papers found that the immobilization effectiveness of biochars for PTEs including As was significantly higher under freeze–thaw aging compared to dry–wet cycle, a result consistent with the result of this study. Importantly, CMBC amendment demonstrated superior immobilization efficiencies for PTEs compared to other modified biochars under both FT- and DW-aging, highlighting its retention durability and remediation potential for PTE-contaminated soil.

3.2.2 The change in fractionation of As

Regardless of the aging processes, CMBC amendment decreased the labile As fractions (F1 + F2) and increased the stable forms (F4 + F5) in both BS and RS soils (Fig. 5a, b), indicating a conversion of mobile As into more immobile species. The reduction in labile As under CMBC amendment was dose-dependent and corresponded to a proportional rise in stable As species. At the 5 wt% CMBC application rate, the combined F4 + F5 fractions increased by 11–32% in BS soil and 39–73% in RS soil across all aging treatments, compared to CK soil. This finding confirms the immobilization effectiveness of CMBC for As, accounting for the decrease in WS-As contents. Notably, the transformation from labile to stable As fractions was consistently higher in RS than in BS, indicating a stronger preference for As immobilization in RS soil, which aligns with the WS-As results. This may be because Al–OH_2^+ groups in RS soil immobilize arsenate (AsO_4^{3-}) through inner-sphere complexation, while

Table 1 Comparison of PTEs immobilization behaviors using biochar-based material amendment under dry–wet and freeze–thaw cycle aging

Material	Soil type	Dose (wt%)	Aging type	Contaminant	Immobilization efficiency (%)	Aging mechanism	References
$KMnO_4$-modified biochars	Red soil	6	Dry–wet cycle	Cd	52	Increasing the O-containing functional groups and complexation with Cd	Meng et al. (2022)
			Freeze–thaw cycle		56	Accelerating the ion exchange between Mn and Cd due to the Mn loss	
Wheat straw biochar	Alkaline soil	5	Dry–wet cycle	Cd	14.6	Increasing the O-containing functional groups, providing more binding site for Cd	Yang et al. (2021)
				Ni	17.0		
			Freeze–thaw cycle	Cd	12.9	Formation of new carbonate minerals promotes Cd precipitation	
				Ni	13.0		
Zero-valent iron-embedded biochar	Red soil	5	Dry–wet cycle	As	78	Oxidation dissolution of ZVI and the formation of mobile reduced As(III)	Zhang et al. (2022a, b)
			Freeze–thaw cycle		91	Crystallization of amorphous iron adsorbed As and oxidation of As(III) to As(V)	
Magnesium–aluminum modified biochar	Yellow soil	1	Dry–wet cycle	As	−1	The dissolution of O-containing functional groups	Peng et al. (2023)
				Cd	22		
			Freeze–thaw cycle	As	19	Increasing the hydrotalcite structure	
				Cd	24		
Wood sawdust biochar	Tailings black soil	5	Dry–wet cycle	As	−46	Increasing the lignin content of biochar and thus promotes Pb immobilization	Kim et al. (2024)
				Pb	61		
			Freeze–thaw cycle	As	−50	Decreasing the biochar stability and high DOM release, thereby enhancing As and Pb mobilities	
				Pb	12		
Fe-biochar	Red soil	3	Dry–wet cycle	As	39	Decreasing the residual fractions of As and Cr	Wang et al. (2023a, b)
				Cr	95		
			Freeze–thaw cycle	As	50	Promoting the conversion of amorphous to crystalline Fe bound As and Cd	
				Cr	99		
Ce-Mn modified biochar	Red soil	5	Dry–wet cycle	As	95	Dispersed biochar-soil microparticles induce moderate Fe/Ce–O-As complexation and less As(III) oxidation	This study
			Freeze–thaw cycle		99	More Ce/Si nano-bridge mediated CMBC-soil colloid adhesion enhances Fe/Ce–O-As complexation and As(0) formation	
	Black soil		Dry–wet cycle		92	Dispersed biochar-soil microparticles decrease Fe/Ce–O-As complexation and As(III) oxidation	
			Freeze–thaw cycle		94	Ce/Si nano-bridge mediated CMBC-soil colloid adhesion enhances Fe/Ce–O-As complexation and As(III) oxidation	

organic matter in BS soil competes for adsorption sites, thereby reducing As immobilization efficiency (Cao et al. 2025). The divergence may involve differences in crystal structures, functional group types, and coordination fates between the two soils, with the molecular mechanism requiring further confirmation by specific characterization techniques.

The migration coefficient (MC) serves as a key indicator to assess the mobilization properties of PTEs in soil. As illustrated in Fig. 5c, d, the MC values of As in CMBC-amended soils under different aging treatments generally followed the order: NA > DW > FT. The significantly lower ($p < 0.05$) MCs under FT-aging imply a redistribution process of As species in soil. This is supported by a 10–15% increase in the fractions of As bound to well crystalline Fe-Al oxide and residual species in FT-aged soils compared to NA- and DW-aged samples. The geochemical transformation of As derived from above phenomena likely occurs in two stages. First, upon CMBC application and incubation, a portion of As species is converted from active fractions (e.g., nonspecifically and specifically-sorbed As) to metastable species associated with poorly crystalline Fe/Al oxide-bound As. Second, FT-aging promotes the further transformation of these metastable phases into highly stable forms, such as well crystalline Fe/Al oxide-bound and residual As species, with this stabilization being more pronounced in RS than in BS. This FT-driven stabilization mechanism can be ascribed to the enhanced formation of $As_nMn_{(1-n)}(OH)_3$ precipitation

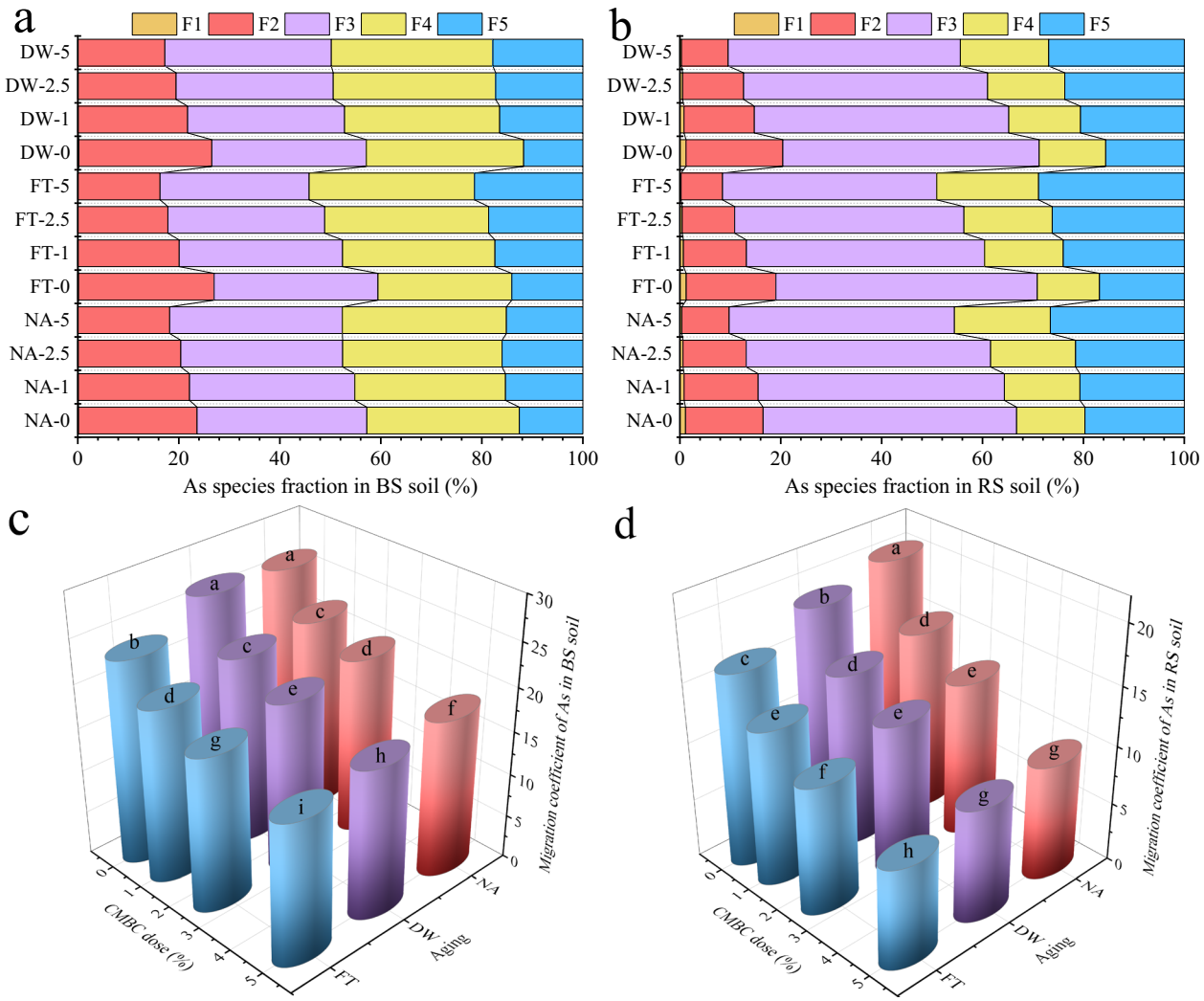

Fig. 5 Species distribution and migration coefficients of As in **a**, **c** BS and **b**, **d** RS soils with or without CMBC amendment under different aging treatments. The NA, DW, and FT denote natural, dry–wet cycle, and freeze–thaw cycle aging, respectively and their adjunct numbers (0, 1, 2.5, and 5) indicate CMBC addition doses (%). F1: nonspecifically sorbed As; F2: specifically-sorbed As; F3: poorly crystalline Fe and Al oxide-bound As; F4: well crystalline Fe and Al oxide-bound As; F5: residual As

and As-Mn/Ce complexation via multiple edge-sharing corner coordination in CMBC-amended soil under FT-aging (Wang et al. 2023a). Similar aging-induced immobilization has been reported for other PTEs. For example, the phytoavailable Cd in soil amended with wheat straw biochar was reduced by > 10% under FT-aging compared to NA- and DW-aging, which was attributed to an increase in O-containing functional groups on biochar that provided additional binding sites for Cd retention (Yang et al. 2021). Furthermore, MgO-modified palygorskite biochar (MPBC) exhibited enhanced Cd immobilization under combined FT- and DW-aging relative to either aging treatment alone, as the synergistic aging accelerated MPBC oxidization by citric acid, thereby promoting Cd-π complexation, ion exchange, and precipitation (Yang et al. 2024a).

3.3 Relationship analysis between As immobilization and soil properties

As mentioned above, CMBC amendment effectively enhances As immobilization through the changes in soil properties such as pH reduction and increased DOC and AP contents. This suppression of As mobilization subsequently increases soil enzyme activities by reducing As toxicity. However, the strength of these interactions varies considerably with soil type and aging processes. To quantify these relationships, we constructed Pearson correlation matrices to evaluate the linkages between As

mobilization parameters (e.g., WS-As, F1-F2 fractions) and key soil properties in CMBC-amended soils subjected to different aging treatments.

As shown in Fig. S1, soil pH in RS soil exhibited a significant positive correlation with As mobilization parameters (WS-As: r = 0.78–0.97, $p < 0.05$; F1/F2 fractions: r = 0.79–0.95, $p < 0.05$), whereas these correlations became insignificantly ($P > 0.05$) in BS soil. This suggests that As mobilization in RS soil is more sensitive to pH variation, likely due to the pH-dependent dissolution of Fe/Mn-(oxyhydr)oxides. Under weakly acidic condition (pH < 6.5), partial dissolution of amorphous Fe/Mn phases can expose more available binding sites for As sequestration through surface complexation (Yang et al. 2024b). Furthermore, a stronger negative correlation was observed in BS soil (r = −0.44 to −0.87) than in RS soil (r = −0.10 to −0.65) between DOC content and As mobilization indices. The greater influence of DOC on As stabilization in BS soil may be related to its richer abundance of O-containing functional groups and low-molecular-weight organic acids, which are characteristic of Phaeozem-derived BS. These organic matters can be adsorbed onto CMBC and release humic-like lignin and tannin, which act as electron shuttles to mediate microbial reduction of Fe(III) (oxyhydr)oxides, thereby influencing As complexation and redox processes (Si et al. 2024; Wu et al. 2019).

Interestingly, AP exhibited a consistent negative correlation (r = −0.47 to −0.97, $p < 0.05$) with As mobilization indices across all soil types and aging treatments, demonstrating that phosphate-mediated As fate by CMBC amendment is independent of soil type and aging pattern. This universal correlation suggests the robust effectiveness of CMBC in As immobilization under complex DW- and FT-cycle perturbations, which can be attributed to multiple immobilization mechanisms including As-Mn/Ce complexation and As-mineral-bearing precipitation that can overcome the phosphate competition. Similarly, the four enzyme activities also showed consistent negative correlations (r = −0.22 to −0.91) with As mobilization indices across soil types and aging treatments, indicating that CMBC-mediated As detoxification universally enhanced microbial activity.

3.4 Potential ecological effects of Ce/Mn in CMBC material

The introduction of Ce and Mn through modified biochar warrants consideration of their potential ecological impacts. As an essential plant micronutrient, Mn participates in key redox processes and can form oxide barriers on root surfaces, thereby reducing the uptake of PTEs like Cd (Wang et al. 2025). Ce, a rare earth element, may influence soil enzyme activities and nutrient cycling. Previous studies have reported that nano-CeO_2 showed least toxicity to crops like wheat and cucumber in agricultural soil, while increasing soil enzyme activities and root biomass (Chen et al. 2023; Xie et al. 2022). But CeO_2 has also been shown to cause root oxidative stress and decrease nutrient components such as vitamin C and soluble sugar (Xie et al. 2022), indicating its context-dependent ecological influence.

The ecological risks of these introduced metals are closely linked to their concentrations and environmental mobilities (Kurian 2020). In this study, Ce and Mn within the CMBC matrix were primarily stabilized as crystalline phases (e.g., CeO_2, MnO_2) and incorporated into soil-biochar aggregates via Ce-Si nano-bridging, which limited their bioavailability and leaching potential. Leaching tests further confirmed that the released levels of Ce and Mn from CMBC-amended soils ranged from 30 to 45 mg kg^{-1} and from 0.10 to 0.22 mg kg^{-1}, respectively (Fig. S6), both of which are far below their natural background values (Ce: 60–85 mg kg^{-1}; Mn: 400–500 mg kg^{-1}) (Chen et al. 2023). Given that Ce/Mn exhibit minimal mobility and a dual nature of effect, including both plant growth promotion and potential stress, we therefore conclude that these two metals in aged soils pose minimal ecological risks. However, the long-term behavior of slowly released metals from biochar and their comprehensive effects on plants and microorganisms require further investigation.

3.5 Aging mechanisms of CMBC for As immobilization in BS and RS soils

3.5.1 The changes in micro/nano-interface between CMBC and soil particle under different aging processes

The micro-interfacial patterns between CMBC and soil particles under various aging processes were investigated using SEM–EDS analysis. Aging treatments significantly modified the morphologies and key elemental compositions of CMBC. As shown in Fig. S2, the pristine CMBC exhibited a typical scale-like, fragmented porous structure (Fig. S2a) with a gully-like surface coated with flaky agglomerates of Ce/Mn nanoparticles (Fig. S2b), consistent with the prominent Ce and Mn signals in the corresponding EDS spectrum (Fig. S2c). In contrast, aged CMBC recovered from both BS and RS soils displayed reduced porosity, with partial pore occlusion by soil microparticles (Fig. 6). Compared to the relatively smooth surfaces in NA-aged CMBC (Fig. 6a, e), DW- and FT-aged CMBC exhibited rougher morphologies accompanied by pore collapse, particularly in BS soil. These structural changes indicate that DW/FT-aging fragmented the carbon skeleton of CMBC surfaces and thus increased its SSA from 140 m^2 g^{-1} to 156–198 m^2 g^{-1} due to intense temperature-humidity fluctuations (Table S2). This finding aligns with previous report that

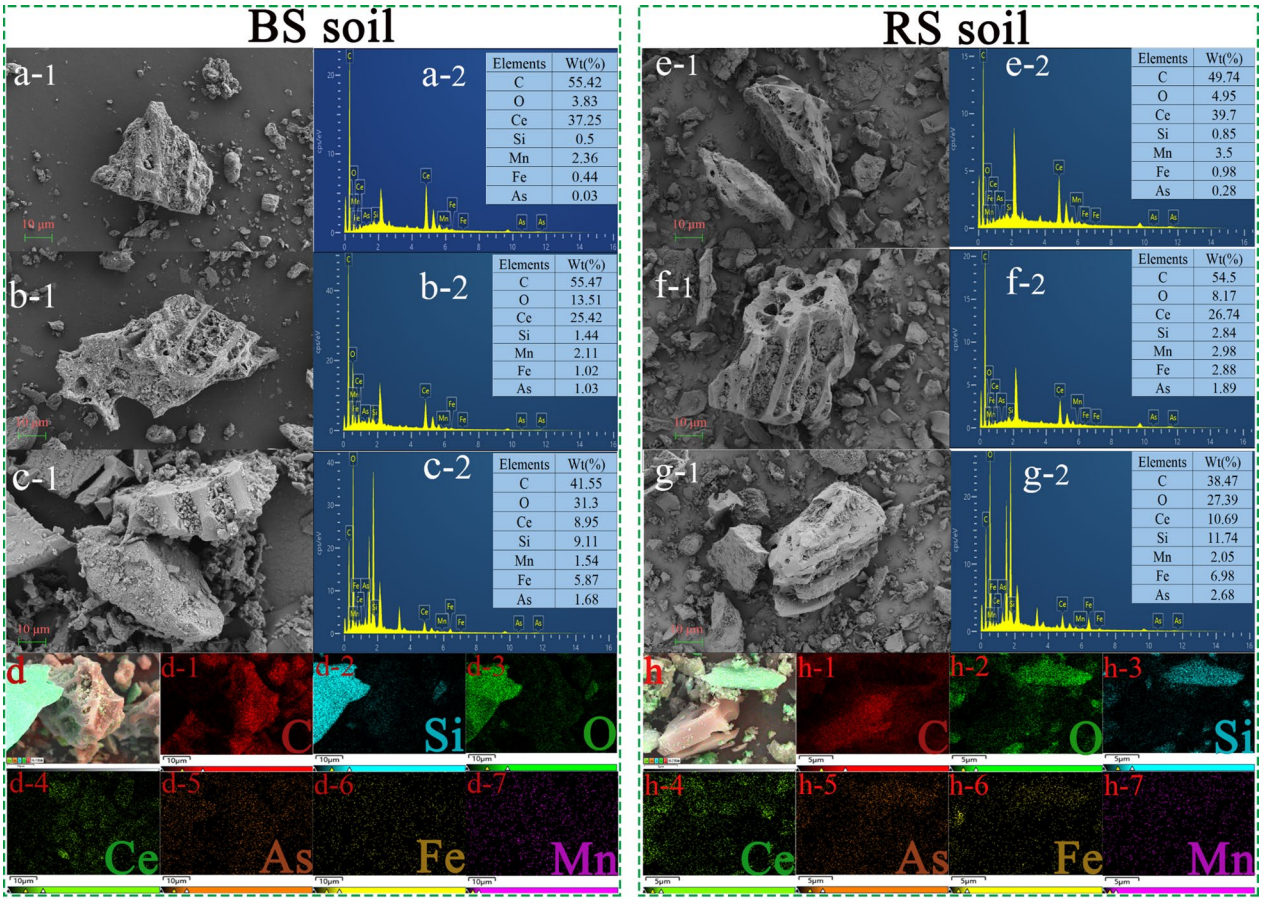

Fig. 6 SEM–EDS images of aged CMBC in BS and RS soils, for its morphology patterns and accompanied EDS spectra after **a-1/2**, **e-1/2** NA-aging, **b-1/2**, **f-1/2** DW-aging, and **c-1/2**, **g-1/2** FT-aging in both soils. EDS mapping of element distribution on interface between FT-aged CMBC and soil microparticle in both soils, for the images of **d**, **h** all elements, **d-1**, **h-1** C element, **d-2**, **h-3** Si element, **d-3**, **h-2** O element, **d-4**, **h-4** Ce element, **d-5**, **h-5** As element, **d-6**, **h-6** Fe element, and **d-7**, **h-7** Mn element

DW- and FT-aging disrupted biochar porosity, consequently enhancing SSA through structural degradation (Yang et al. 2024a). Interestingly, CMBC aged in RS soil retained more intact porous structures (Fig. 6e1–g1) than that aged in BS soil (Fig. 6a1–c1). This divergence may correlate with textural differences: RS soil contained substantially higher clay content (25.5%) than BS soil (9.7%) (Table S1). We hypothesize that clay minerals with smaller particle sizes preferentially occupy macropores and mesopores in biochar via hydraulic transport, as evidenced by the elevated Si/Fe signals in EDS spectra of RS soil (Fig. 6e2–g2). Such pore-filling effects may provide structural reinforcement against collapse induced by temperature-humidity cycling (Ravindiran et al. 2024). Paradoxically, despite the expected SSA reduction from pore occlusion, CMBC aged in RS soil showed higher SSA than that recovered from BS soil (Table S2). This discrepancy may be attributed to the limited pore filling of micropores in CMBC by clay minerals and cellulose/hemicellulose degradation during aging, which in turn potentially generates new micropores (Zhao and Shang 2023). The detailed interplay between these processes requires further study.

The aging processes resulted in an obvious depletion of Ce and Mn mass ratios on CMBC, with the extents of loss following the order: FT-aging > DW-aging > NA-aging in both soils (Fig. 6a2–c2, e2–g2). This suggests that FT-cycling preferentially triggers the partial Ce/Mn dissolution, likely driven by acid-enhanced mineral solubilization under soil pH reduction (Fig. 1c, d). Although such dissolution may theoretically impair As immobilization by weakening Ce/Mn-As complexation, our results of WS-As and As fractionation revealed a contradictory decrease in As mobilization. The incompatible outcome can be due to the doping of Fe-(oxyhydr)oxide on FT-aged CMBC surfaces through solute transport, as confirmed by the significantly increased Fe mass ratios in EDS spectra (Fig. 6c2, g2). Biogenic Fe(III/II)-(oxyhydr)

oxides are key regulators of PTE geochemical cycling and are particularly effective in immobilizing As via As-Fe complexation and $FeAsO_4$ coprecipitation in soil systems (Lyu et al. 2023). The observed 4- to 8-fold enrichment of As on FT-aged CMBC (EDS spectra in Fig. 6c2, g2) strongly supports this hypothesis, demonstrating a net enhancement in As adsorption that partially explains the preferential immobilization during FT-aging.

Notably, SEM images revealed marked microstructural differences in aged CMBC across the various treatments: NA- and DW-aged samples exhibited separate and dispersed microparticles, whereas FT-aged samples formed dense aggregates of nonporous particles with distinct Si–C fluorescence boundaries in EDS mapping (Fig. 6d1–d7, h1–h7). This demonstrates that freeze–thaw cycling induces tight adhesion between soil microparticles and biochar substrates, a novel phenomenon attributable to ice-mediated interfacial interactions. This microstructural reorganization likely arises from frost-heaving and thaw-settlement cycles, which generate soil fragments with higher surface energy that exhibit strong molecular attraction to biochar via hydrophilic interactions (Yang et al. 2019; Zuo et al. 2022). Such colloid-microparticle adhesion further promotes As sequestration through physical entrapment. To elucidate this mechanism, we characterized the nano-interfacial interactions between soil and CMBC colloids under freeze–thaw conditions.

TEM images of FT-aged CMBC revealed the aggregation of soil nanoparticles on the CMBC surfaces (Fig. 7a, f), which was confirmed by clear Si–C fluorescence boundaries in EDS mappings (Fig. 7e1–e7, j1–j7), consistent with SEM–EDS results. In contrast, NA- and DW-aged CMBC samples maintained discrete particles devoid of soil attachment (Fig. S3a, S3d), underscoring that FT-aging uniquely drives interfacial adhesions between soil and CMBC. In the enlarged views (Fig. 7b, g), a zigzag-shaped crack appeared at FT-aged CMBC-soil interface and distributed micropores were observed within the carbon layer, whereas NA- and DW-aged samples retained a denser biochar structure (Fig. S3b, S3e). These structural alterations suggest that FT cycling generates additional micropores in CMBC, which accounts for its increased SSA despite partial pore occlusion by Si/Fe-minerals. Such carbon matrix fragmentation corroborates our hypothesis that intense freeze–thaw cycles drive morphological transformation of CMBC from bulk to micro/nanoscale architectures. High-resolution TEM (HRTEM) images of the carbon-soil interface revealed fuzzy band-like separation planes (marked by grey lines in Fig. 7c, h). Fourier calculations of the intercalated lattice fringes at the interface indicated spacings of 2.702 nm in BS soil (Fig. 7d) and 3.170 nm in RS soil (Fig. 7i), corresponding to the (112) plane of $CeSiO_2$ and the (−121) plane of Ce_2SiO_5, respectively, consistent with the XRD results. These Ce-Si crystals act as nano-bridges that connect nano-CMBC to soil particles and further promote As immobilization via adsorption onto Fe/Mn-(oxyhydr)oxides, as evidenced by the uniform distribution of Fe, Mn, and As in EDS mappings (Fig. 7e5–e7, j5–j7). Interestingly, the interface in BS exhibited a wider separation (Fig. 7c) than that in RS soil (Fig. 7h), while RS interfaces contained more intercalated Ce-Si crystals, reflecting tighter soil colloid-CMBC adhesion in RS. This closer interface likely strengthens As binding through increased van der Waals forces and hydrogen bonds with active Fe/Mn minerals and O-containing functional groups, while also providing greater mechanical resistance to As-associated crystal defects (Shen et al. 2022). Herein, we further analyzed the changes in crystal structures and coordination fates of key species for As immobilization at CMBC-soil interface under different aging processes.

3.5.2 Changes in key crystal structures of CMBC under different aging processes

The crystalline structures of CMBC under different aging treatments were characterized via XRD analysis. As shown in Fig. 8a, the primary crystalline phases in pristine CMBC were CeO_2, MnO_2, and SiO_2. After aging in BS soil, the crystalline phases of CMBC remained largely unchanged, except for a newly emerged peak at 27.946° belonging to Ce_2SiO_5 (JCPDS PDF 48-0054) in the FT-aged sample (see local enlargement in Fig. S4), consistent with TEM observations. In contrast, aging in RS soil induced significant phase transformation, as evidenced by the appearance of diffraction peaks at 11.513° for $CaSiO_3$ (JCPDS PDF 29-0372) and at 33.179° and 35.651° for Fe_2O_3 (JCPDS PDF 89-8103). These newly formed Ca/Fe-oxides likely originated from the intercalation of Ca/Fe-rich minerals released from RS soil into the delaminated CMBC structure, occurring under the conditions of intense temperature-humidity fluctuations (Feng et al. 2025). The presence of these reactive metal oxides is correlated with enhanced As sequestration, as further demonstrated by a unique peak at 43.138° assigned to FeAs (JCPDS PDF 77-1359).

Notably, characteristic CeO_2 diffraction peaks at 28.549°, 33.077°, and 56.342° were absent in RS-aged CMBC, which may be due to the acidic pH and elevated Eh of Krasnozem soil. Under such hydrated oxidizing conditions, Ce-minerals tend to undergo amorphization, resulting in the formation of amorphous Ce-oxides with enhanced As-binding capacity (Kurian 2020). This interpretation is supported by the detection of a diffraction peak at 31.221° belonging to Ce_4As_3 (JCPDS PDF 89-3223), which was exclusively found in FT-aged CMBC

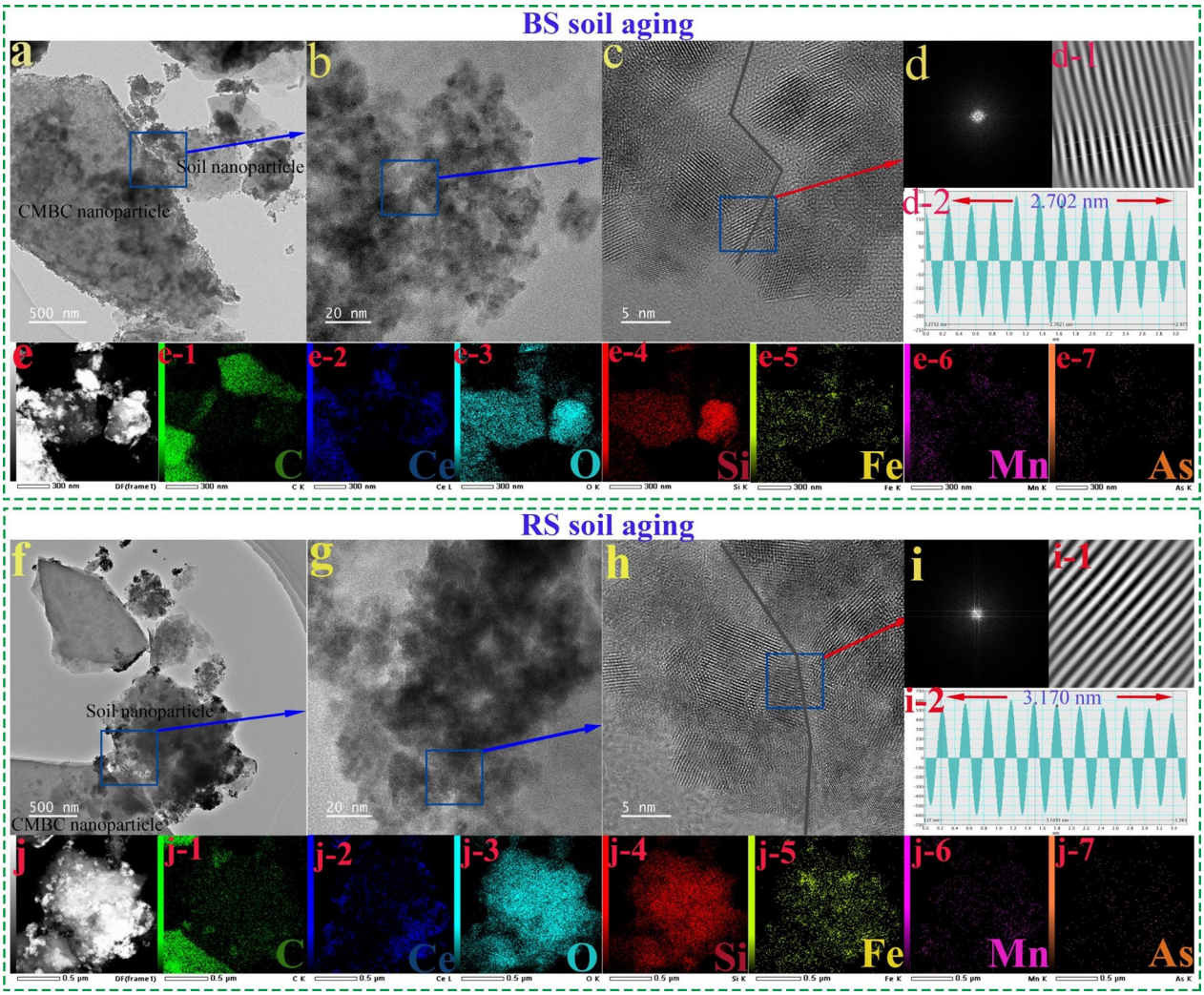

Fig. 7 TEM-EDS images of CMBC under FT-aging in both soils, for **a**, **f** representational adhesion images of aggregates between soil and CMBC nanoparticles. Correspondingly **b**, **g** enlarged images and **c**, **h** their HRTEM images in both soils. Lattice profile of HRTEM images descripting the nanointerface between soil and nano-CMBC, for **d**, **i** crystal diffraction pattern, **d-1**, **i-1** lattice fringe pattern, and **d-2**, **i-2** lattice spacing pattern. EDS elemental distribution between nano-CMBC and soil particle in both soils under FT-aging, for the images of **e**, **j** diffraction pattern of the selected region, **e-1**, **j-1** C element, **e-2**, **j-3** Ce element, **e-3**, **j-2** O element, **e-4**, **j-4** Si element, **e-5**, **j-5** Fe element, **e-6**, **j-6** Mn element, and **e-7**, **j-7** As element

from RS soil. These additional Ce/Fe-bound As species further elucidates the preference for As immobilization in RS soil. Interestingly, a distinct peak at 27.946° associated with $CeSi_2$ (JCPDS PDF 06-0485) was also identified in FT-aged CMBC in RS soil, similar to that observed in BS soil. This provides crystallographic evidence for the nano-bridging interactions between nano-CMBC and soil microparticles as revealed by TEM analysis.

3.5.3 Changes in coordination fates of key functional groups on CMBC under different aging processes

FT-IR spectra (Fig. 8b) were employed to track changes in the surface functional groups of CMBC across different aging treatments. Apparently, the stretching vibration peaks of O-containing functional groups, such as phenolic –OH at 3421 cm^{-1} and lactone COO– at 1430 cm^{-1}, exhibited significantly increased intensities on aged CMBC compared to the pristine one. The most pronounced enhancement was observed for COO– group in RS-aged CMBC. These findings indicate that soil aging promotes the enrichment of O-containing functional groups on CMBC, which is further supported by the substantially elevated (–OH)/(C=O) ratio, an index of surface O-containing functional group abundance (Table S2). This phenomenon likely stems from oxidative disconnection and transformation of aromatic moieties

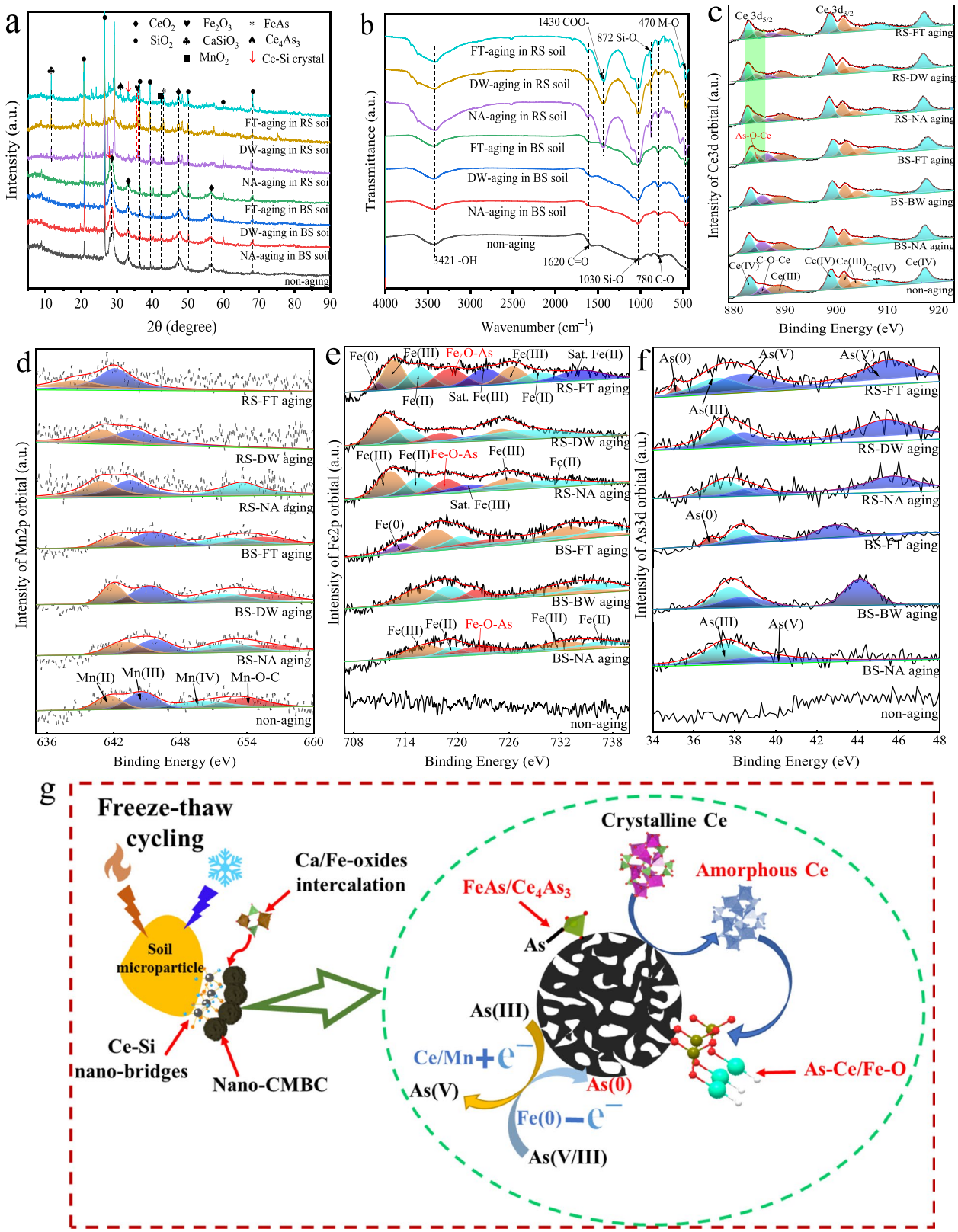

Fig. 8 **a** XRD patterns and **b** FT-IR spectra of CMBC subjected to different aging processes in both soils. High resolution XPS spectra of deconvoluted **c** Ce 3d, **d** Mn 2p, **e** Fe 2p, and **f** As 3d spectra for different aged CMBC in both soils. **g** Effect mechanisms of freeze–thaw cycling on As fate in the interface between soil microparticle and nano-CMBC particle

in CMBC into O-bearing components such as hydroxyl and carbonyl groups (Wang and Liu 2024). Additionally, bending vibration peaks at 470 cm^{-1} and 780 cm^{-1} were attributed to M–O (M = Ce, Fe, or Ca) and C–O groups, respectively. The ratio of (M–O)/(C–O) serves as a metric of metal group abundance. Remarkably, both the (M–O)/(C–O) and (–OH)/(C = O) ratios in CMBC increased in the order: FT-aging > DW-aging > NA-aging (Table S2), suggesting preferential grafting of metal- and oxygen-groups onto FT-aged CMBC surface. This trend aligns with SEM–EDS and XRD results. The synergistic enrichment of these additional metal- and oxygen-groups on FT-aged CMBC favors As complexation. Therefore, the coordination fate of As with key functional groups on aged CMBC was further investigated via XPS characterization.

According to the aforementioned studies, Ce-, Mn-, and Fe-metal oxides play critical roles in As bonding during CMBC aging. Hence, high resolution XPS spectra of O 1 s (Fig. S5), Ce 3d (Fig. 8c), Mn 2p (Fig. 8d), and Fe 2p (Fig. 8e) were analyzed for CMBC aged under different conditions. The O 1 s spectra of all aged CMBC were deconvoluted into three components: C–O, C = O, and M–O (M = Ce, Mn, or Fe) bonds. Notably, a new peak at ~ 533 eV, belonged to As–O, was detected only in RS soil-aged CMBC but was absent in BS soil-aged samples. This As–O bond exhibited the highest peak area and relative proportion in FT-aged CMBC (Table S3), indicating an enhanced formation of stable As-associated species on FT-aged CMBC surface in RS soil, consistent with the XRD results. Crucially, the O-bonded peaks shifted toward higher binding energies (BEs) after aging in BS soil, whereas aging in RS soil induced a shift to lower BEs. Similar BE shifts were observed in deconvoluted peaks of Ce 3d (Fig. 8c), Mn 2p (Fig. 8d), and Fe 2p (Fig. 8e). These contrasting BE trends likely reflect distinct metal speciation mechanisms in the two soils. BS soil, rich in organic ligands, may promote electron withdrawal from metal ions via chelation, thereby increasing oxidation states and BEs of redox-active metals. In contrast, RS soil is characterized by a high abundance of positively charged goethite and hematite, which can adsorb oxidized As while accepting electrons, thereby reducing BEs (Dong et al. 2025). This conjecture is supported by the emergent Fe $2p_{3/2}$ and Fe $2p_{1/2}$ doublet (Fig. 8e), in which both Fe(III) and Fe(II) species were detected in all aged CMBC samples. Correspondingly, the stoichiometric ratio of Fe(IIII): Fe(II) decreased from 1.2 to 1.5 in BS-aged samples to 1.1–1.4 in RS-aged samples (Table S6), confirming greater ferric reduction in RS soil, a process that facilitates electron access during redox reactions. Furthermore, an Fe–O–As bond was identified in deconvoluted Fe 2p spectra of all aged CMBC samples (but not in pristine CMBC), emphasizing the pivotal role of Fe-oxides in As immobilization during aging. The relative proportion of Fe–O–As bonds was highest in FT-aged CMBC in both soils (Table S6), corroborating the unique As–Fe crystalline phase observed by XRD and indicating that FT-aging preferentially promotes As stabilization. Besides that, Ce species also contributed significantly to As sequestration. In Fig. 8c, the Ce 3d spectra revealed a peak near 884 eV, attributable to Ce–O–As bond, which was present in RS-aged CMBC samples and FT-aged BS samples. This demonstrates that both host Ce-oxides and intercalated guest Fe-oxides on the CMBC surface synergistically drive As retention.

Similar to Fe 2p analysis, the Ce 3d spectra of all CMBC were deconvoluted into Ce(IV) and Ce(III) valence states. The calculated stoichiometric Ce(IV): Ce(III) ratios compared as the order: non-aging > DW-aging > NA-aing > FT-aging (Table S4), indicating an enhanced reduction of Ce(IV) to Ce(III) during FT-aging. A parallel trend was observed in the Mn 2p spectra (Fig. 8d), where the relative abundance of higher-valence Mn species declined, as reflected by the Mn(IV): [Mn(III) + Mn(II)] ratios: non-aging > NA-aing > DW-aging ≈ FT-aging in BS soil, and non-aging > NA-aing > DW-aging > FT-aging in RS soil (Table S5). The prominent reduction of redox-active Ce/Mn on aged-CMBC surfaces, particularly under FT-aging, can induce As(III) oxidation via coupled reactions from $2Mn(Ce)O_2 + e^- + 6H^+ \rightarrow 2Mn(Ce)OOH + 2H_2O$ to $AsO_3^{3-} + H_2O \rightarrow AsO_4^{3-} + e^- + 6H^+$ (Lyu et al. 2024a). In agreement with this mechanism, the As 3d spectra (Fig. 8f) revealed adsorbed As signals at ~ 37 eV (AsIII), ~ 38 eV (AsV), and ~ 45 eV (AsV). The As(III): As(V) ratios compared sequentially: NA-aging (1.25) > DW-aging (0.52) > FT-aging (0.45) in BS soil, and NA-aging (0.33) > DW-aging (0.30) > FT-aging (0.26) in RS soil (Table S7). This inverse correlation between the extent of Ce/Mn reduction and the proportion of As(III) confirms the Ce/Mn-driven As(III) oxidation, where FT-aging exerted the strongest redox effect. Notably, characteristic peaks of As(0) emerged exclusively in FT-aged CMBC at 36.8 eV in BS soil and 35.1 eV in RS soil (Wang et al. 2023b). This signifies a secondary geochemical process of As, that is the partial reduction of As(V)/As(III) to inert As(0) in a frozen anaerobic environment caused by the supply of protons from Fe(0) on CMBC surface (Zhang et al. 2022b). The additional peaks at 713.69 eV for BS soil and 710.82 eV for RS soil confirmed the formation of highly reactive Fe(0) on FT-aged CMBC (Fig. 8e), which drives the reduction and transformation to As(0) via two possible pathways: $2Fe^0 + 4H^+ + 2HAsO_3^{2-} \rightarrow Fe_2O_3 + 2As^0 + 3H_2O$ and $4Fe^0 + 6H^+ + 2H_2AsO_3^- \rightarrow 2Fe_2O_3 + 4As^0 + 6H_2O$. This finding is similar with previous studies demonstrating

that As(0) can be trapped between an Fe(0) core and an Fe(III) oxide outer shell under anoxic conditions (Tuček et al. 2017).

In summary, as displayed in Fig. 8g, FT-cycling uniquely induces the formation of tight adhesion between soil microparticles and CMBC matrix via Ce–Si crystal nano-bridges, in contrast to the dispersed microparticles observed in NA/DW-aged samples. This interfacial restructuring promotes the intercalation of Ca/Fe-oxides and amorphous Ce-oxides into CMBC, facilitating the formation of As–Fe/Ce crystalline phases. Concurrently, synergistic enrichment of metal- and oxygen-groups on FT-aged CMBC surface induces the formation of stable As–Ce/Fe–O species while enabling dual redox transformation: (1) Ce/Mn reduction drives bulk As(III) oxidation to As(V), and (2) Fe(0) oxidation mediates partial transformation of As(V)/As(III) to inert As(0). Importantly, aged-CMBC shows a preference for As immobilization in RS soil, where tighter adhesion between nano-CMBC and RS colloids amplifies the bonding of Ce/Fe-oxides with As and intensifies the oxidation of As(III) to As(V) through heightened participation of Ce/Mn reduction.

4 Conclusion

This study investigated the aging behavior of CMBC in two As-contaminated soils under three aging treatments. Overall, CMBC amendment most effectively altered soil properties under FT-aging, followed by DW-aging and NA-aging, after 30 aging cycles by reducing pH while increasing DOC, AP, and four enzyme activities. Concurrently, CMBC significantly reduced water-soluble As concentrations and mobilization coefficients, with FT-aging exhibiting superior immobilization. This enhanced performance under FT-aging is attributed to Ce–Si crystal nano-bridges that tightly adhere soil microparticles to CMBC matrix, which promotes Ca/Fe-oxide intercalation and amorphous Ce-oxides formation within CMBC, thereby facilitating As–Fe/Ce crystalline phase development. Meanwhile, synergistic metal–oxygen groups enrichment on FT-aged CMBC surface enables stable As–Ce/Fe–O formation and induces dual redox transformation: (1) Ce/Mn reduction oxidizes As(III) to As(V), and (2) Fe(0) oxidation reduces As(V)/As(III) to inert As(0). Interestingly, CMBC exhibited preferential As immobilization in RS soil due to tighter CMBC-RS colloid adhesion, which amplifies bonding of Ce/Fe-oxides with As and intensifies As(III) oxidation by raised Ce/Mn reduction. Our findings regarding the freeze–thaw-driven transformation of As offer a new perspective for understanding the migration and transformation of toxic elements in cold-region environments, such as high-latitude and high-altitude areas.

Supplementary Information

The online version contains supplementary material available at https://doi.org/10.1007/s42773-026-00573-4.

Supplementary material 1.

Acknowledgements
This work was financed by National Natural Science Foundation of China (No. 42377257) and National Key Technology Research and Development Program of China (2020YFC1806401).

Author contributions
Peng Lyu: Conceptualization; Methodology; Formal analysis and investigation; Writing—original draft preparation. Xiaoya Huang: Methodology; Formal analysis and investigation. Lianfang Li: Methodology; Funding acquisition; Resources; Supervision. Yan Jiao: Resources; Methodology. The authors read and approved the final manuscript.

Funding
This work was financed by National Natural Science Foundation of China (No. 42377257) and National Key Technology Research and Development Program of China (2020YFC1806401).

Data availability
The datasets used or analyzed during the current study are available from the corresponding author on reasonable request.

Declarations

Competing interests
No competing financial interests exist.

Author details
[1]Inner Mongolia Engineering Center for Regional Resource Utilization and Eco-Environmental Protection, College of Chemistry and Environmental Science, Inner Mongolia Normal University, Hohhot 010022, China. [2]Key Laboratory of Agriculture and Rural Eco-Environment, Ministry of Agriculture and Rural Affairs, Institute of Environment and Sustainable Development in Agriculture, Chinese Academy of Agricultural Sciences, Beijing 100081, China.

Received: 1 July 2025 Revised: 15 December 2025 Accepted: 7 January 2026
Published online: 16 February 2026

References

Cao T, Chen W, Yang T, He T, Liu Z, Meng J (2017) Surface characterization of aged biochar incubated in different types of soil. Bioresour 12(3):6366–6377. https://doi.org/10.15376/biores.12.3.6366-6377

Cao J, Liu Y, Liu Y, Xue S, Xiong H, Xu C, Xu Q, Duan G (2025) Predicting the efficiency of arsenic immobilization in soils by biochar using machine learning. J Environ Sci 147:259–267. https://doi.org/10.1016/j.jes.2023.11.016

Chen D, Lin Z, Ai F, Xia Y, Du W, Yin Y, Guo H (2023) Divergent responses and ecological risks of wheat (*Triticum aestivum* L.) to cerium oxide nanoparticles in different soil types. Sci Total Environ 860:160429. https://doi.org/10.1016/j.scitotenv.2022.160429

Cooper JA, Malakar A, Kaiser M (2023) Self-functionalization of soil-aged biochar surfaces increases nitrate retention. Sci Total Environ 861:160644. https://doi.org/10.1016/j.scitotenv.2022.160644

Cowie AL (2023) Biochar as a fast track to net zero. Nat Food. https://doi.org/10.1038/s43016-023-00714-z

Dong M, Jiang M, He L, Zhang Z, Gustave W, Vithanage M, Niazi NK, Chen B, Zhang X, Wang H, He F (2025) Challenges in safe environmental

applications of biochar: identifying risks and unintended consequence. Biochar 7(1):12. https://doi.org/10.1007/s42773-024-00412-4
Feng Z, Li J, Chen N, Feng C (2025) Sulfonated corn stalk enhanced hydrogel adsorption for heavy metal from metal mine gallery effluent. Sep Purif Technol 357:130160. https://doi.org/10.1016/j.seppur.2024.130160
Gong H, Zhao L, Rui X, Hu J, Zhu N (2022) A review of pristine and modified biochar immobilizing typical heavy metals in soil: applications and challenges. J Hazard Mater 432:128668. https://doi.org/10.1016/j.jhazmat.2022.128668
Gong Y, Hou R, Fu Q, Li T, Wang J, Su Z, Shen W, Zhou W, Wang Y, Li M (2024) Modified biochar reduces the greenhouse gas emission intensity and enhances the net ecosystem economic budget in black soil soybean fields. Soil till Res 237:105978. https://doi.org/10.1016/j.still.2023.105978
Guo Z, Lu Z, Liu Z, Zhou W, Yang S, Lv J, Wei M (2024) Difference in the effect of applying *Bacillus* to control tomato Verticillium wilt in black and red soil. Microorganisms 12(4):797. https://doi.org/10.3390/microorganisms12040797
Guo P, Gu X, Li Z, Xu X, Cao Y, Yang G, Kuang C, Li X, Qing Y, Wu Y (2025) A novel almond shell biochar modified with FeS and chitosan as adsorbents for mitigation of heavy metals from water and soil. Sep Purif Technol 360:130943. https://doi.org/10.1016/j.seppur.2024.130943
Honma T, Ohba H, Kaneko-Kadokura A, Makino T, Nakamura K, Katou H (2016) Optimal soil Eh, pH, and water management for simultaneously minimizing arsenic and cadmium concentrations in rice grains. Environ Sci Technol 50(8):4178–4185. https://doi.org/10.1021/acs.est.5b05424
Kim HB, Kim JG, Alessi DS, Baek K (2024) Temporal changes in the mobility of As, Pb, Zn, and Cu due to differences in biochar stability caused by lignin content. Chem Eng J 493:152567. https://doi.org/10.1016/j.cej.2024.152567
Kurian M (2020) Cerium oxide based materials for water treatment – a review. J Environ Chem Eng 8(5):104439. https://doi.org/10.1016/j.jece.2020.104439
Liang T, Li L, Zhu C, Liu X, Li H, Su Q, Ye J, Geng B, Tian Y, Sardar MF, Huang X, Li F (2020) Adsorption of As(V) by the novel and efficient adsorbent cerium-manganese modified biochar. Water 12(10):2720. https://doi.org/10.3390/w12102720
Liao X, Mao S, Gao W, Wang S, Hu J, Malghani S (2025) Risk of increasing soil nitrous oxide emissions by chemical oxidation modification on biochar. J Environ Manage 375:124336. https://doi.org/10.1016/j.jenvman.2025.124336
Liu X, He Y, Li J, Li J, Zhang J, Tang X (2025) Does biochar field aging reduce the kinetic retention for weakly hydrophobic antibiotics in purple soil? Biochar 7(1):69. https://doi.org/10.1007/s42773-025-00460-4
Long XX, Yu ZN, Liu SW, Gao T, Qiu RL (2024) A systematic review of biochar aging and the potential eco-environmental risk in heavy metal contaminated soil. J Hazard Mater 472:134345. https://doi.org/10.1016/j.jhazmat.2024.134345
Luo L, Wang J, Lv J, Liu Z, Sun T, Yang Y, Zhu YG (2023) Carbon sequestration strategies in soil using biochar: advances, challenges, and opportunities. Environ Sci Technol 57(31):11357–11372. https://doi.org/10.1021/acs.est.3c02620
Lyu P, Li L, Huang X, Xie J, Ye J, Tian Y, Huang J, Zhu C (2023) Ternary Ca–Mg–Al layered double-hydroxides for synergistic remediation of As, Cd, and Pb from both contaminated soil and groundwater: characteristics, effectiveness, and immobilization mechanisms. J Hazard Mater 442:130030. https://doi.org/10.1016/j.jhazmat.2022.130030
Lyu P, Li L, Huang J, Ye J, Zhu C (2024a) Magnetic biochar-supported layered double hydroxide for simultaneous remediation of As and Cd in soil: effectiveness, retention durability, and insight into a new immobilization mechanism. J Clean Prod 434:140136. https://doi.org/10.1016/j.jclepro.2023.140136
Lyu P, Li L, Zhou X, Huang J, Ye J, Liu X, Xie J, Wang Z (2024b) Modification of arsenic and cadmium species and accumulation in rice using biochar-supported iron-(oxyhydr)oxide and layered double hydroxide: insight from Fe plaque conversion and nano-bioassembly in the root. Chem Eng J 494:152847. https://doi.org/10.1016/j.cej.2024.152847
Manasa MRK, Katukuri NR, Darveekaran Nair SSS, Haojie Y, Yang Z, Guo RB (2020) Role of biochar and organic substrates in enhancing the functional characteristics and microbial community in a saline soil. J Environ Manage 269:110737. https://doi.org/10.1016/j.jenvman.2020.110737
Meng Z, Huang S, Laird DA, Wu J, Lin Z (2022) Identifying key processes driving Cd long-term adsorption and immobilization by biochar in soils and evaluating combined aging effects under simulated local climates. J Environ Chem Eng 10(6):108636. https://doi.org/10.1016/j.jece.2022.108636
Peng C, Gong K, Li Q, Liang W, Song H, Liu F, Yang J, Zhang W (2023) Simultaneous immobilization of arsenic, lead, and cadmium in soil by magnesium-aluminum modified biochar: influences of organic acids, aging, and rainfall. Chemosphere 313:137453. https://doi.org/10.1016/j.chemosphere.2022.137453
Ravindiran G, Rajamanickam S, Janardhan G, Hayder G, Alagumalai A, Mahian O, Lam SS, Sonne C (2024) Production and modifications of biochar to engineered materials and its application for environmental sustainability: a review. Biochar 6(1):62. https://doi.org/10.1007/s42773-024-00350-1
Saraugi SS, Asare F, Gazo R, Routray W (2025) Advances in sustainable production of biochar and biochar-based nanocomposites: a critical review. J Clean Prod 514:145752. https://doi.org/10.1016/j.jclepro.2025.145752
Shao P, Yin H, Li Y, Cai Y, Yan C, Yuan Y, Dang Z (2023) Remediation of Cu and As contaminated water and soil utilizing biochar supported layered double hydroxide: mechanisms and soil environment altering. J Environ Sci 126:275–286. https://doi.org/10.1016/j.jes.2022.05.025
Shen B, Wang H, Xiong H, Chen X, Bosch EGT, Lazic I, Qian W, Wei F (2022) Atomic imaging of zeolite-confined single molecules by electron microscopy. Nature 607(7920):703–707. https://doi.org/10.1038/s41586-022-04876-x
Si D, Song Wu, Wu H, Wang D, Fu QL, Wang Y, Wang P, Zhao FJ, Zhou D (2024) Activated carbon application simultaneously alleviates paddy soil arsenic mobilization and carbon emission by decreasing porewater dissolved organic matter. Environ Sci Technol 58(18):7880–7890. https://doi.org/10.1021/acs.est.4c00748
Sun Y, Xiong X, He M, Xu Z, Hou D, Zhang W, Ok YS, Rinklebe J, Wang L, Tsang DCW (2021) Roles of biochar-derived dissolved organic matter in soil amendment and environmental remediation: a critical review. Chem Eng J 424:130387. https://doi.org/10.1016/j.cej.2021.130387
Sun H, Luo L, Wang J, Wang D, Huang R, Ma C, Zhu YG, Liu Z (2022) Speciation evolution of phosphorus and sulfur derived from sewage sludge biochar in soil: ageing effects. Environ Sci Technol 56(10):6639–6646. https://doi.org/10.1021/acs.est.2c00632
Tuček J, Prucek R, Kolařík J, Zoppellaro G, Petr M, Filip J, Sharma VK, Zbořil R (2017) Zero-valent iron nanoparticles reduce arsenites and arsenates to As(0) firmly embedded in core-shell superstructure: challenging strategy of arsenic treatment under anoxic conditions. ACS Sustain Chem Eng 5(4):3027–3038. https://doi.org/10.1021/acssuschemeng.6b02698
Wang M, Liu Q (2024) Interactions between nanobiochar and arsenic: effects of biochar aging methods on arsenic binding capacity and mechanisms. Environ Pollut. https://doi.org/10.1016/j.envpol.2024.125105
Wang L, O'Connor D, Rinklebe J, Ok YS, Tsang DCW, Shen Z, Hou D (2020) Biochar aging: mechanisms, physicochemical changes, assessment, and implications for field applications. Environ Sci Technol 54(23):14797–14814. https://doi.org/10.1021/acs.est.0c04033
Wang G, Liu F, Tariq M, Wan J, Liang W, Zhang W, Peng C, Yang J (2022) A comparative study on various indicators for evaluating soil health of three biochar materials application. J Clean Prod 343:131085. https://doi.org/10.1016/j.jclepro.2022.131085
Wang L, Luo Y, Pang J, Li Y, Wu H, Jiang X, Tong J, Shi J (2023a) Fe-biochar for simultaneous stabilization of chromium and arsenic in soil: rational design and long-term performance. Sci Total Environ 862:160843. https://doi.org/10.1016/j.scitotenv.2022.160843
Wang S, Liao P, Cen L, Cheng H, Liu Q (2023b) Biochar promotes arsenopyrite weathering in simulated alkaline soils: electrochemical mechanism and environmental implications. Environ Sci Technol 57(22):8373–8384. https://doi.org/10.1021/acs.est.2c09874
Wang Z, Zhao H, Shi Z, Zhao H, Chen S, Chen Z, Yuan Y, Zhang C, Jia B, Jia H (2025) Manganese dioxides induce the transformation and protection of dissolved organic matter simultaneously: a significance of crystallinity. Environ Sci Technol 59(2):1222–1231. https://doi.org/10.1021/acs.est.4c10054
Wei B, Zhang D, Jeyakumar P, Trakal L, Wang H, Sun K, Wei Y, Zhang X, Ling H, He S, Wu H, Huang Z, Li C, Wang Z (2024) Iron-modified biochar effectively mitigates arsenic-cadmium pollution in paddy fields: a meta-analysis. J Hazard Mater 469:133866. https://doi.org/10.1016/j.jhazmat.2024.133866

Wenzel WW, Kirchbaumer N, Prohaska T, Stingeder G, Lombi E (2001) Arsenic fractionation in soils using an improved sequential extraction procedure. Anal Chim Acta 436(2):309–323. https://doi.org/10.1016/S0003-2670(01)00924-2

Wu X, Bowers B, Kim D, Lee B, Jun YS (2019) Dissolved organic matter affects arsenic mobility and iron(iii) (hydr)oxide formation: implications for managed aquifer recharge. Environ Sci Technol 53(24):14357–14367. https://doi.org/10.1021/acs.est.9b04873

Xie C, Guo Z, Zhang P, Yang J, Zhang J, Ma Y, He X, Lynch I, Zhang Z (2022) Effect of CeO_2 nanoparticles on plant growth and soil microcosm in a soil-plant interactive system. Environ Pollut 300:118938. https://doi.org/10.1016/j.envpol.2022.118938

Xu Z, Xu X, Tsang DCW, Cao X (2018) Contrasting impacts of pre- and post-application aging of biochar on the immobilization of Cd in contaminated soils. Environ Pollut 242:1362–1370. https://doi.org/10.1016/j.envpol.2018.08.012

Xu D, Ni X, Kang J, He B, Zuo Y, Mosa AA, Yin X (2024) Mechanisms of cadmium adsorption by ramie nano-biochar with different aged treatments. Appl Soil Ecol. https://doi.org/10.1016/j.apsoil.2023.105175

Yadav V, Jain S, Mishra P, Khare P, Shukla AK, Karak T, Singh AK (2019) Amelioration in nutrient mineralization and microbial activities of sandy loam soil by short term field aged biochar. Appl Soil Ecol 138:144–155. https://doi.org/10.1016/j.apsoil.2019.01.012

Yang W, Shang J, Li B, Flury M (2019) Surface and colloid properties of biochar and implications for transport in porous media. Crit Rev Environ Sci Technol 50(23):2484–2522. https://doi.org/10.1080/10643389.2019.1699381

Yang K, Wang X, Cheng H, Tao S (2021) Effect of aging on stabilization of Cd and Ni by biochars and enzyme activities in a historically contaminated alkaline agricultural soil simulated with wet-dry and freeze-thaw cycling. Environ Pollut 268:115846. https://doi.org/10.1016/j.envpol.2020.115846

Yang K, Wang X, Cheng H, Tao S (2023) Effects of physical aging processes on the bioavailability of heavy metals in contaminated site soil amended with chicken manure and wheat straw biochars. Environ Pollut 324:121414. https://doi.org/10.1016/j.envpol.2023.121414

Yang K, Guo B, Shen K, Luo W, Zhang B, Hua Y, Zhang Y (2024a) Unraveling immobilization mechanisms of Cd in soil by MgO-modified palygorskite/biochar composite: DFT calculation and combined-artificial aging. J Environ Manage 370:122576. https://doi.org/10.1016/j.jenvman.2024.122576

Yang Y, Liu T, Borch T, Fang L, Hu S, Chi W, Chen G, Cheng K, Wang Q, Li X, Yuan X, Li F (2024b) Iron biogeochemical redox cycling dominantly controls cadmium availability in acidic paddy soils. Geochim Cosmochim Acta 378:186–202. https://doi.org/10.1016/j.gca.2024.06.029

Yuan Y, Li J, Wang C, An G (2021) Contrasting microcystin-LR sorption and desorption capability of different farmland soils amended with biochar: effects of biochar dose and aging time. Environ Pollut 286:117364. https://doi.org/10.1016/j.envpol.2021.117364

Zhang P, Fan J, Xu X, Xu Z, Yu Y, Zhao L, Qiu H, Cao X (2022a) Contrasting effects of dry-wet and freeze-thaw aging on the immobilization of As in As-contaminated soils amended by zero-valent iron-embedded biochar. J Hazard Mater 426:128123. https://doi.org/10.1016/j.jhazmat.2021.128123

Zhang W, Cho Y, Vithanage M, Shaheen SM, Rinklebe J, Alessi DS, Hou CH, Hashimoto Y, Withana PA, Ok YS (2022b) Arsenic removal from water and soils using pristine and modified biochars. Biochar 4(1):55. https://doi.org/10.1007/s42773-022-00181-y

Zhao K, Shang J (2023) Transport of biochar colloids under unsaturated flow condition: roles of chemical aging and cation type. Sci Total Environ 859:160415. https://doi.org/10.1016/j.scitotenv.2022.160415

Zuo Y, Meng F, Li T, Fu Q, Liu D, Hou R, Li Q, Li M (2022) Effect of biochar application on freezing-thawing deformation of farmland soil during freeze–thaw cycling. Geoderma 405:115510. https://doi.org/10.1016/j.geoderma.2021.115510